NASA TECHNICAL NOTE

NASA TN D-5316

NASA TN D-5316

SUBSONIC AERODYNAMIC CHARACTERISTICS OF A LARGE-SCALE 1.075-PRESSURE-RATIO TIP-TURBINE CRUISE-FAN PROPULSION SYSTEM AT ANGLE OF ATTACK

by Francis J. Capone

Langley Research Center
Langley Station, Hampton, Va.

NATIONAL AERONAUTICS AND SPACE ADMINISTRATION • WASHINGTON, D. C. • AUGUST 1969

SUBSONIC AERODYNAMIC CHARACTERISTICS OF A LARGE-SCALE 1.075-PRESSURE-RATIO TIP-TURBINE CRUISE-FAN PROPULSION SYSTEM AT ANGLE OF ATTACK

By Francis J. Capone

Langley Research Center
Langley Station, Hampton, Va.

NATIONAL AERONAUTICS AND SPACE ADMINISTRATION

For sale by the Clearinghouse for Federal Scientific and Technical Information
Springfield, Virginia 22151 – CFSTI price $3.00

SUBSONIC AERODYNAMIC CHARACTERISTICS OF A LARGE-SCALE 1.075-PRESSURE-RATIO TIP-TURBINE CRUISE-FAN PROPULSION SYSTEM AT ANGLE OF ATTACK

By Francis J. Capone
Langley Research Center

SUMMARY

An investigation has been conducted in the Langley 16-foot transonic tunnel to determine aerodynamic characteristics and pressure distributions of a large-scale 1.075-pressure-ratio tip-turbine cruise fan at angle of attack. The intent of this investigation was to determine trends rather than absolute levels in performance since the fan was originally designed as a low-pressure-ratio lift fan. The gas generator was closely coupled to the fan so that the gas-generator nacelle extended forward and below the fan nacelle. The investigation was conducted at Mach numbers of 0.30, 0.50, and 0.70 and at angles of attack from -2° to 8°. The test Reynolds number based on the fan diameter (91.44 cm) varied from 3.90×10^6 to 11.25×10^6.

Angle-of-attack variation affected only the external pressure distributions at the fan-cowl leading edge. Premature supercritical flow occurred on the fairing between the fan and gas-generator nacelles at angles of attack of 2° and 5° at a Mach number of 0.70, well below the fan-nacelle design Mach number of 0.81. Nacelle minimum drag occurred at an angle of attack of 2° and both the lift and pitching-moment curves were linear over an angle-of-attack range of -2° to 5° throughout the Mach number range of the test.

INTRODUCTION

The National Aeronautics and Space Administration has been conducting extensive research on V/STOL airplanes that utilize tip-turbine-driven lift fans (refs. 1 to 4). These propulsion systems use the exhaust products of a gas generator (turbojet engine) to drive turbine blades mounted around the periphery of a ducted fan. Conversion of the high disk loading of the turbojet gas generator to the lower disk loading of the fan results in an increase in static thrust for the same power input. Reference 2 presents results for a full-scale model of a current VTOL airplane that has a lift fan in each wing, a pitch-control fan mounted in the nose (needed for transitional flight), and a conventional turbojet for cruise. A lift fan can also be used for subsonic cruise by rotating the fan 90° so that it acts essentially as a turbofan engine with a bypass ratio that can vary from 8:1 to 15:1.

In this way, at low forward speeds, the thrust of the driving gas generator is augmented and the specific fuel consumption can be less for the cruise fan than for conventional turbojet or turbofan engines. Reference 3 presents results of a V/STOL transport configuration that has both lift and lift-cruise fan engines. Low-speed results for an isolated 1.1-pressure-ratio lift-cruise fan are presented in reference 5. (Pressure ratio is representative of stagnation pressure rise across fan.)

An investigation concerned with extending cruise-fan internal and external performance to high subsonic Mach numbers was conducted in the Langley 16-foot transonic tunnel. The effects of variation of geometry and exit area were studied at Mach numbers up to 0.85 for eight configurations. These results for eight configurations at an angle of attack of 0° are presented in reference 6. One of the configurations was also tested at angle of attack; the purpose of the present report is to present external aerodynamic characteristics and pressure distributions for this configuration at Mach numbers of 0.30, 0.50, and 0.70 and at angles of attack from -2° to 8°. These results are intended to give performance trends rather than absolute levels since the tip-turbine fan used for this investigation was designed as a lift fan and not as a cruise fan (ref. 6).

SYMBOLS

Model forces and moments are referred to an axis system for which the origin is at the intersection of the fan-rotor reference plane and fan-nacelle center line, as shown in figure 1. A discussion of procedures used to compute nacelle net aerodynamic characteristics is given in the section entitled "Data Reduction" and a complete description of the procedure used to determine the thrust characteristics can be found in appendix A of reference 6. Dimensions for this report are only in the International System of Units whereas in reference 6 they are in both the International System and the U.S. Customary Units.

A_{max} reference area based on fan-nacelle maximum diameter (does not include gas-generator-nacelle cross section), 1.268 meters

C_A axial-force coefficient measured by force balance, $\frac{\text{Axial force}}{q_\infty A_{max}}$

$C_{A,n}$ net axial-force coefficient, $C_A + C_{F,n}$

$C_{D,n}$ net drag coefficient, $C_{A,n} \cos \alpha + C_{N,n} \sin \alpha$

$C_{D,r}$ total ram drag coefficient, $\frac{\text{Ram drag}}{q_\infty A_{max}}$

$C_{F,g}$ gross ideal thrust coefficient, $\frac{\text{Gross thrust}}{q_\infty A_{max}}$

$C_{F,n}$ net thrust coefficient, $C_{F,g} - C_{D,r} \cos \alpha$

$C_{L,n}$ net lift coefficient, $C_{N,n} \cos \alpha - C_{A,n} \sin \alpha$

C_m pitching-moment coefficient measured by force balance, $\frac{\text{Pitching moment}}{q_\infty A_{max} d_{max}}$

$C_{m,n}$ net pitching-moment coefficient, C_m - (Effects of ram drag)

C_N normal-force coefficient measured by force balance, $\frac{\text{Normal force}}{q_\infty A_{max}}$

$C_{N,n}$ net normal-force coefficient, $C_N - C_{D,r} \sin \alpha$

C_p pressure coefficient, $\frac{p_l - p_\infty}{q_\infty}$

$C_{p,sonic}$ pressure coefficient for sonic flow

d_{max} fan-nacelle maximum diameter, 127.00 centimeters

l fan-cowl-plus-afterbody length, 261.90 centimeters

M free-stream Mach number

$\dot{m}_F$ fan-inlet mass-flow rate, kilograms/second

$\dot{m}_E$ gas-generator-inlet mass-flow rate, kilograms/second

N_F fan rotational speed, percent of full speed

p_l local static pressure, newtons/meter^2

p_∞ free-stream static pressure, newtons/meter^2

q_∞ free-stream dynamic pressure, newtons/meter^2

r radius (specific radii are identified in fig. 5), centimeters

$T_{t,\infty}$ free-stream stagnation temperature, ^oK

V_∞ free-stream velocity, meters/second

x	longitudinal distance (in the results presented, x is measured from the fan-nacelle leading edge; in the configuration ordinates (fig. 5), however, x-values are measured as shown in the separate sketches), centimeters
y	vertical distance (specific values of y are indicated in fig. 5), centimeters
α	angle of attack, degrees
θ	meridian angle as defined in figure 2, degrees
$\sqrt{\sigma}$	stagnation temperature correction parameter for corrections to standard sea-level conditions, $\sqrt{T_{t,\infty}}/288.05$

APPARATUS AND PROCEDURE

Model Installation

A simplified sketch of the cruise fan is shown as figure 2 and photographs are given as figure 3. The installation of the model in the Langley 16-foot transonic tunnel and overall model dimensions are shown in figure 4. The model was sting supported so that the fan-nacelle center line was 63.50 centimeters above the tunnel center line. For this investigation, the propulsion system was mounted in an inverted position and all references made to model geometry is according to the wind-tunnel installation. All model geometry is referred to the fan-rotor reference plane, hereinafter referred to as plane 10.3. (This identification of the plane location is consistent with usage established by the engine manufacturer.)

As a means of increasing the structural integrity of the model, guy wires were attached to the sting by two fixtures which protruded out through holes at the rear of the gas-generator nacelle. A flexible seal between the fixtures and the gas-generator nacelle prevented any air leakage. A second set of guy wires was attached directly to the sting downstream of the gas-generator nacelle. (See fig. 3(b).)

Propulsion System

The propulsion system of this model consisted of the X-376 tip-turbine fan (pitch-control fan of ref. 2) driven by a modified T58-GE-6A gas generator.

Fan.- The fan was a single-stage, 1.075-pressure-ratio, tip-turbine-driven fan. The rotor contained 36 fan blades and the tip-mounted turbine buckets. The fan-tip diameter was 91.44 centimeters and the hub diameter was 41.15 centimeters. Design rotational speed of the fan was 4074 revolutions per minute. A bulletnose was provided to

smooth the flow entering the fan. A single set of 52 stator vanes was part of the rear fan frame.

The tip-turbine buckets were located radially outboard on the fan-rotor blade tips. The gas-generator exhaust was admitted through a scroll to the fan-tip turbines. The scroll of this partial-admission turbine covered the lower 167° of the circumferential arc; the remainder of the turbine arc was inactive. The tip-turbine diameter was 105.66 centimeters.

Gas generator.- The gas generator was a modified T58-GE-6A turboshaft gas-turbine engine and used JP-4 as a fuel. The modification to the gas generator consisted of removing the power turbine. Design rotational speed of this gas generator is 26 300 revolutions per minute. A flow-straightening and bellows section was provided between the gas generator and fan scroll. (See fig. 2.) The fan and fan-tip turbine flows were discharged into a common annulus before entering the exhaust-nozzle system. (See fig. 2.)

Configuration Tested

Configuration 113 of reference 6 was tested at angle of attack. The various model components are defined in figure 2 and ordinates are given in figure 5.

Fan cowl and inlet.- The fan cowl and inlet are that portion of the fan nacelle (excluding gas-generator nacelle) that is forward of plane 10.3. (See figs. 2, 4, and 5.) The fan cowl is the external surface whereas the fan inlet is the internal surface. The fan cowl (fig. 5(b)) had a critical design Mach number of 0.81, an NACA inlet designation 1-64-98, and a maximum diameter of 127.00 centimeters at the fan center line. The large diameter was necessary to accommodate the turbine scroll and to keep the nacelle symmetrical. The ratio of the diameter at the fan-inlet leading edge to the inlet-throat diameter was 1.133.

Afterbody, nozzle shroud, and plug.- The afterbody is that part of the fan nacelle that is rearward of plane 10.3, the internal contour being defined as the nozzle shroud. (See figs. 2 and 5(b).) The external contour of the afterbody was a circular-arc segment $\left(r/d_{max} = 5.25\right)$ terminating with a boattail angle of 12°. (See fig. 5(b).)

The nozzle shroud consisted of a cold and a hot side. (See fig. 5(b).) The cold side consisted of the upper 173° of the shroud and the hot side the remaining 187°. The hot side was fabricated to allow for expansion due to the heating effects of the fan-turbine flow. The flow splitter of the same radius as the shroud cold side and located circumferentially at the same position as the hot side was provided in order that fan-turbine exhaust-gas pressure and temperature could be measured before mixing occurred with the cold fan flow. The nozzle-shroud internal angle at the exit was 11.5°.

The nozzle plug (fig. 5(d)) provided the configuration with an exit area of 2793 square centimeters and was sized for fan operation at a Mach number of 0.80. The plug half-angle was 12.5°.

Gas-generator nacelle and inlet.- The gas-generator nacelle is defined as the external surface of the fairing enclosing the gas generator, force balance, and sting up to the flexible seal (fig. 2). The gas-generator inlet is the internal surface up to the gas-generator compressor face. The gas-generator-nacelle design critical Mach number was 0.81 and the NACA inlet designation was 1-50-110. Ordinates for the gas-generator nacelle and inlet are presented in figure 5(e), and the bulletnose ordinates are given in figure 5(f). The flexible seal insured no leakage between the end of the gas-generator nacelle and the nacelle-to-sting transition section which was attached to the sting (fig. 2).

Instrumentation

Model forces were measured with a six-component internally located strain-gage balance. An externally wrapped water jacket was used around the balance to maintain a constant balance temperature. Up to 485 pressures were measured and recorded on 12 pressure-scanning devices, each capable of scanning 48 pressures. Each pressure-scanning device contained a single pressure transducer. The outputs of the force balance and pressure-scanning units were digitized and recorded on punch cards. A portion of the pressure instrumentation was used for determining static-pressure distributions over the various model surfaces. The remainder of the pressure instrumentation was used for measuring flow conditions at the various instrumentation planes throughout the model as described in reference 6.

Gas-generator and fan-turbine exhaust stagnation temperatures were measured with chromel-alumel thermocouple probes and recorded on continuous strip-chart recorders. Gas-generator rotational speed was measured with a tachometer generator, and fan rotational speed was determined from a variable-reluctance magnetic pickup. The gas-generator fuel mass-flow rate was determined from calibration curves based on corrected inlet mass-flow rate for the T58-GE-6A gas generator. In addition, gas-generator fuel and oil pressure, gas-generator and fan vibration, fan-blade stresses, and nacelle-cavity temperatures were monitored continually to insure safe operation.

Wind Tunnel and Tests

The investigation was conducted in the Langley 16-foot transonic tunnel, which is a single-return atmospheric wind tunnel with a slotted, octagonal test section. The speed range of this tunnel is from a Mach number of 0.20 to 1.30. This investigation was conducted at Mach numbers of 0.30, 0.50, and 0.70 and at angles of attack of -2°, 0°, 2°, 5°,

and 8° over a range of power settings from windmill to maximum obtainable gas-generator power.

The following procedure was used in recording data. First, the wind tunnel was brought to the desired speed and a windmill data point was taken. The gas generator was started and brought to the idling condition (about 55 to 60 percent maximum speed) and another data point was taken. Then three power-on data points were taken, the last being usually at approximately maximum uncorrected gas-generator speed (usually 98 to 101 percent). About 30 seconds was required to record a data point because of the pressure-scanning equipment used.

Boundary-layer transition strips were not affixed to any portions of the model during the investigation.

CORRECTIONS AND DATA REDUCTION

Corrections

No corrections for wind-tunnel wall interference or blockage effects were applied to the data. The magnitude of these corrections is believed to be negligible, since comparisons of windmill pressure distributions for one configuration (123) and a 1/5-scale flow-through model of the same configuration reported in reference 6 showed good agreement.

Axial force was corrected to the condition of free-stream static pressure acting across the flexible seal. This correction varied from -0.002 to 0.005 in terms of flexible-seal force coefficient $\left(\text{Seal force}/q_{\infty}A_{max}\right)$.

Quoted angles of attack are to be considered as nominal since no corrections for either tunnel flow angularity or model deflection due to load have been made. Flow angularity in the Langley 16-foot transonic tunnel averages about 0.1° upflow.

Data Reduction

A complete description of the performance calculations at $\alpha = 0^{\circ}$ is given in reference 6. The method used to remove the effects of thrust and to arrive at the nacelle net aerodynamic-force coefficients is now described.

The gross ideal thrust was defined in reference 6 as the sum of the ideal thrust computed from pressure measurements at stations (instrumentation planes) just behind the fan tip-turbine discharge and fan discharge. These calculations included frictional losses up to these measuring stations but did not include the frictional losses in the nozzle itself, because the pressure instrumentation was located just behind the fan stators. Thus, the net nacelle-drag measurements presented herein are considered conservative since they include these losses that are usually charged to the internal performance of the propulsion system.

Total ram drag coefficient is defined as

$$C_{D,r} = \frac{V_\infty(\dot{m}_F + \dot{m}_E)}{q_\infty A_{max}} \tag{1}$$

and the system net thrust coefficient at $\alpha = 0^o$ is then simply

$$C_{F,n} = C_{F,g} - C_{D,r} \tag{2}$$

From figure 1, the forces measured directly by the balance along the body axis are noted to be

$$C_N = C_{N,n} + C_{D,r} \sin \alpha \tag{3}$$

$$C_A = C_{A,n} - C_{F,n} \tag{4}$$

where $C_{N,n}$ and $C_{A,n}$ are the nacelle net aerodynamic forces along the body axis and the net thrust coefficient at angle of attack is

$$C_{F,n} = C_{F,g} - C_{D,r} \cos \alpha \tag{5}$$

Solving equations (3) and (4) for the net aerodynamic coefficients along the body axis and converting to a wind axis gives as the nacelle net lift and drag coefficients:

$$C_{L,n} = C_{N,n} \cos \alpha - C_{A,n} \sin \alpha \tag{6}$$

$$C_{D,n} = C_{A,n} \cos \alpha + C_{N,n} \sin \alpha \tag{7}$$

At $\alpha = 0^o$, $C_{D,n} = C_{D,\pi}$ where $C_{D,\pi}$ is defined as a nacelle drag coefficient in reference 6. Substitutions can be made for $C_{N,n}$ and $C_{A,n}$ so that the equations (6) and (7) for $C_{L,n}$ and $C_{D,n}$ can be expressed in terms of the measured balance forces and computed fan net thrust and ram drag.

The net nacelle pitching-moment coefficient can then be obtained by subtracting out the contributions due to the ram drag (ram drag assumed to be acting at the nacelle inlet)

$$C_{m,n} = C_m - \frac{124.46}{d_{max}}(C_{D,r})_F \sin \alpha - \frac{258.95}{d_{max}}(C_{D,r})_E \sin \alpha - \frac{73.66}{d_{max}}(C_{D,r})_E \cos \alpha \tag{8}$$

where

$$\left(C_{D,r}\right)_F = \frac{V_\infty \dot{m}_F}{q_\infty A_{max}} \qquad \text{(Fan ram drag)} \qquad (9)$$

$$\left(C_{D,r}\right)_E = \frac{V_\infty \dot{m}_E}{q_\infty A_{max}} \qquad \text{(Gas-generator ram drag)} \qquad (10)$$

$$C_{D,r} = \left(C_{D,r}\right)_F + \left(C_{D,r}\right)_E \qquad \text{(Total ram drag)} \qquad (11)$$

The constants are simply moments for the respective components of the ram drag and d_{max} = 127.00 centimeters. The dimensions of the moment arms are indicated in figure 4.

RESULTS AND DISCUSSION

Pressure Distributions

The pressure coefficients of figures 6 to 14 have been plotted as a function of x/l where l is the fan-cowl length plus afterbody length (261.90 cm) and the origin of the coordinate system is at the leading edge of the fan cowl. At this point $x = 0$ and x is measured positively to the rear.

Fan-nacelle pressure distributions are presented in figures 6 to 8. The outer surface corresponds to the fan cowl and afterbody, and the inner surface corresponds to the fan inlet and nozzle shroud. Only data at windmill and maximum obtainable fan rotational speed are presented.

Only the external pressure distributions at the fan-cowl lip show any significant effect of angle-of-attack variation. As angle of attack is increased at a given Mach number, cowl-lip suction at $\theta = 0^o$ is greatly reduced, whereas the suction at $\theta = 135^o$ to 150^o is increased. There is essentially no change at $\theta = 90^o$. At $M = 0.70$, the onset of supercritical flow along the fairing section between the fan and gas-generator nacelles at $\alpha = 2^o$ and 5^o (figs. 8(c) and 8(d)) lowers the critical Mach number from that for which the cowl was designed and can be a source of high interference drag due to possible flow separation along the fairing. Reference 6 showed the nacelle critical Mach number was reduced from 0.81 (design to 0.79 at the $\theta = 0^o$ meridian plane and to about 0.71 along the fairing ($\theta = 150^o$). At $\alpha = 5^o$ and $\theta = 150^o$, the nacelle critical Mach number is about 0.65. Although the results at $\alpha = 0^o$ along $\theta = 0^o$ would indicate that isolated nacelle design techniques are adequate, results at the other meridian stations indicate that care must be used for fairing sections that would be similar to that used in the present investigation.

Fan bulletnose and plug pressure distributions are shown in figures 9 to 11. Little or no effect of angle of attack occurs over the Mach number range of the tests. From

reference 6, plug thrust coefficients (based on integration of pressures over external portion of plug) vary from about 0.02 to 0.04.

Gas-generator nacelle and inlet pressure distributions are presented in figures 12 to 14. Increasing angle of attack affected these pressure distributions similarly to those described for the fan nacelle. That is, a decrease of nacelle lip suction at $\theta = 0^{\circ}$ and an increase at $\theta = 180^{\circ}$. The large negative pressure peaks at $\theta = 135^{\circ}$ and 180° at windmill are due to spillage of almost the entire gas-generator streamtube. (Gas-generator mass-flow rate varies from about 1 kilogram per second at windmill to about 8 kilograms per second at maximum power.) There is also nonuniformity to this flow spillage due to windmilling. For example, at $\alpha = 0^{\circ}$ for all Mach numbers, the pressure at the nacelle leading edge is positive at $\theta = 0^{\circ}$ whereas at $\theta = 180^{\circ}$, large negative pressure peaks indicate a rapid acceleration of the flow over this portion of the gas-generator nacelle. (See figs. 12(b), 13(b), and 14(b).) Increasing angle of attack results in much higher negative pressure peaks. Variation of angle of attack had little or no effect along the cylindrical portion of the nacelle (at $\theta = 180^{\circ}$ and $x/l > 0$).

Aerodynamic Characteristics

The variation of measured balance-force coefficients (thrust effects not removed) with corrected fan speed are presented as figure 15. Because of the low-pressure-ratio fan, the net thrust decreases so much as the free-stream Mach number increases that the drag of the system is greater than the net thrust at $M > 0.5$. (See also ref. 6.) Figure 16 shows the variation of net thrust coefficient and total ram drag coefficient with corrected fan speed. In the quantity $C_{D,r} \cos \alpha$, both ram drag and net thrust are shown acting along the same axis, where the sum $C_{F,n} + C_{D,r} \cos \alpha$ is equal to the gross ideal thrust coefficient $C_{F,g}$. Variation of angle of attack is seen to have little or no effect on net thrust coefficient. Hence, there was no effect on fan internal performance over the angle-of-attack range of the tests.

The variation of fan-nacelle net aerodynamic forces (effects of thrust removed) with corrected fan speed are presented as figure 17. These results show that minimum nacelle drag occurred at $\alpha = 2^{\circ}$ for all test Mach numbers. Both nacelle lift and pitching-moment curves are linear up to $\alpha = 5^{\circ}$ at all Mach numbers for a constant corrected fan speed. Nacelle lift-curve slope over this angle-of-attack range varied from about 0.016 to 0.022.

CONCLUDING REMARKS

An investigation has been conducted in the Langley 16-foot transonic tunnel to determine external aerodynamic characteristics and pressure distribution of a large-scale

tip-turbine cruise fan at angle of attack. The investigation was conducted at Mach numbers of 0.30, 0.50, and 0.70 and at angles of attack from -2^{o} to 8^{o}. The test Reynolds number based on the fan diameter (91.44 cm) varied from 3.90×10^{6} to 11.25×10^{6}.

Angle-of-attack variation affected only the external pressure distributions at the fan-cowl leading edge. Premature supercritical flow occurred on the fairing between the fan and gas-generator nacelles at angles of attack of 2^{o} and 5^{o} at a Mach number of 0.70, well below the fan-nacelle design Mach number of 0.81. Nacelle minimum drag occurred at an angle of attack of 2^{o}, and both the lift and pitching-moment curves were linear over an angle-of-attack range of -2^{o} to 5^{o} throughout the Mach number range of the test.

Langley Research Center,
National Aeronautics and Space Administration,
Langley Station, Hampton, Va., April 10, 1969,
721-03-00-02-23.

REFERENCES

1. Hickey, David H.; and Hall, Leo P.: Aerodynamic Characteristics of a Large-Scale Model With Two High Disk-Loading Fans Mounted in the Wing. NASA TN D-1650, 1963.

2. Kirk, Jerry V.; Hickey, David H.; and Hall, Leo P.: Aerodynamic Characteristics of a Full-Scale Fan-in-Wing Model Including Results in Ground Effect With Nose-Fan Pitch Control. NASA TN D-2368, 1964.

3. Hall, Leo P.: Hickey, David H.; and Kirk, Jerry V.: Aerodynamic Characteristics of a Large-Scale V/STOL Transport Model With Lift and Lift-Cruise Fans. NASA TN D-4092, 1967.

4. Chambers, Joseph R.; and Grafton, Sue B.: Static and Dynamic Longitudinal Stability Derivatives of a Powered 0.18-Scale Model of a Fan-in-Wing VTOL Aircraft. NASA TN D-4322, 1968.

5. Giulianetti, Demo J.; Biggers, James C.; and Corsiglia, Victor R.: Wind-Tunnel Test of a Full-Scale, 1.1 Pressure Ratio, Ducted Lift-Cruise Fan. NASA TN D-2498, 1964.

6. Capone, Francis J.; and Norton, Harry T., Jr.: Subsonic Performance Characteristics of a Large-Scale 1.075-Pressure-Ratio Tip-Turbine Cruise-Fan Propulsion System. NASA TN D-5314, 1969.

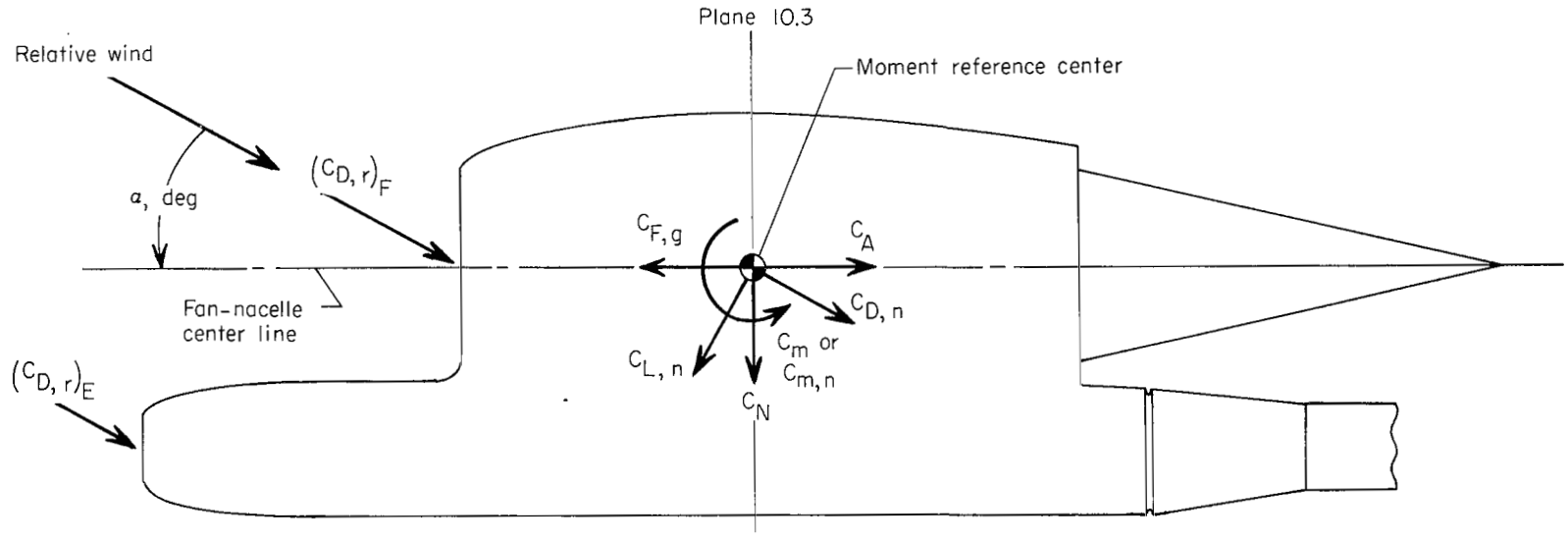

Gross balance forces:

$$C_N = C_{N,n} + C_{D,r} \sin \alpha$$

$$C_A = C_{A,n} - C_{F,n}$$

where:

$$C_{D,r} = (C_{D,r})_F + (C_{D,r})_E$$

$$C_{F,n} = C_{F,g} - C_{D,r} \cos \alpha$$

Nacelle net aerodynamic forces:

$$C_{L,n} = C_{N,n} \cos \alpha - C_{A,n} \sin \alpha$$

$$C_{D,n} = C_{A,n} \cos \alpha + C_{N,n} \sin \alpha$$

Nacelle net pitching moment:

$$C_{m,n} = C_m - (C_m)_{C_{D,r}}$$

where $(C_m)_{C_{D,r}}$ is moment due to total ram drag

Figure 1.- Definition of cruise-fan axis system, force, and moment coefficients showing positive directions as model was mounted in the wind tunnel.

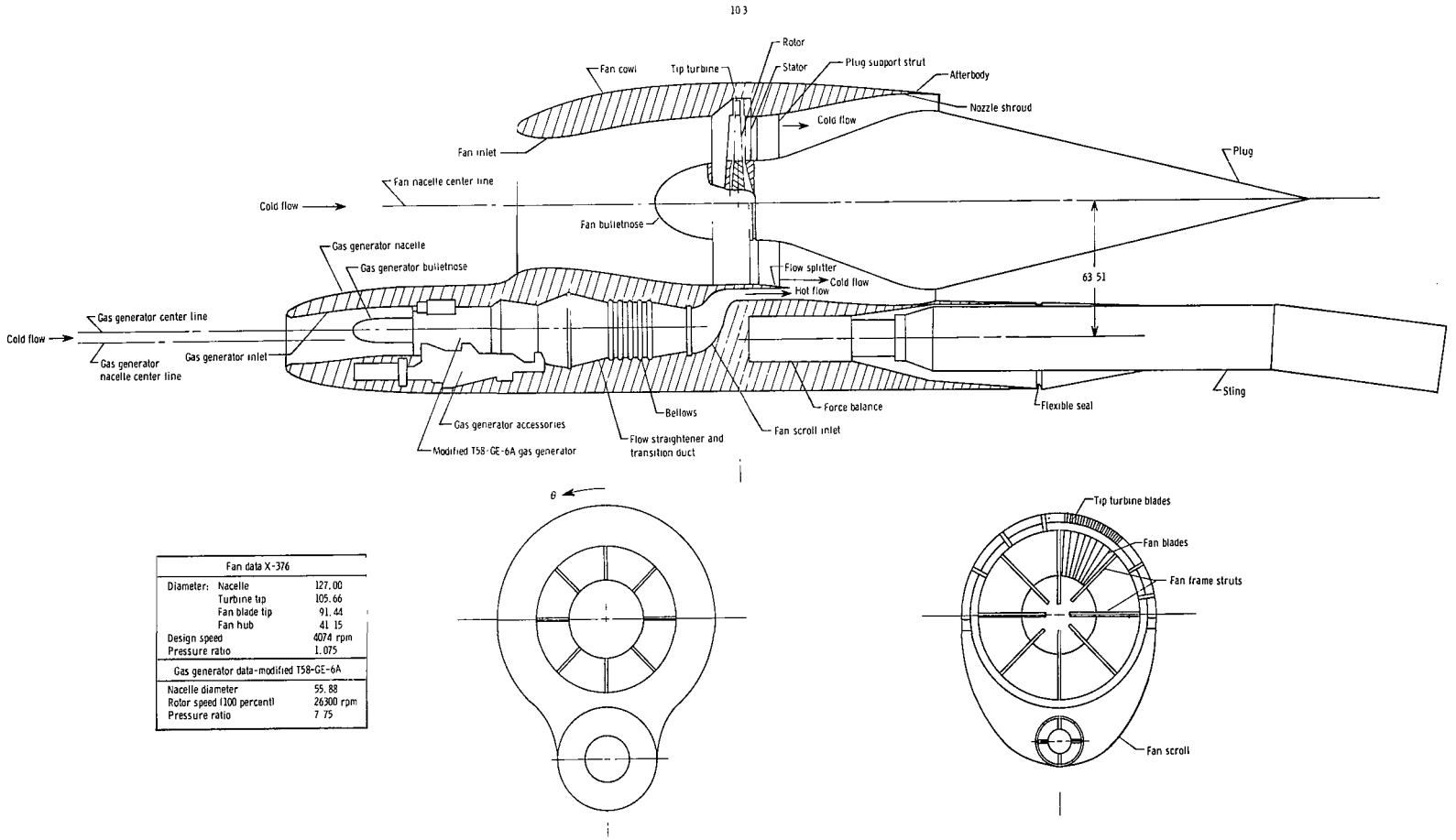

Fan data X-376		
Diameter:	Nacelle	127.00
	Turbine tip	105.66
	Fan blade tip	91.44
	Fan hub	41.15
Design speed		4074 rpm
Pressure ratio		1.075
Gas generator data-modified T58-GE-6A		
Nacelle diameter		55.88
Rotor speed (100 percent)		26300 rpm
Pressure ratio		7.75

Figure 2.- Sketch of cruise fan assembly. All dimensions in centimeters unless otherwise noted.

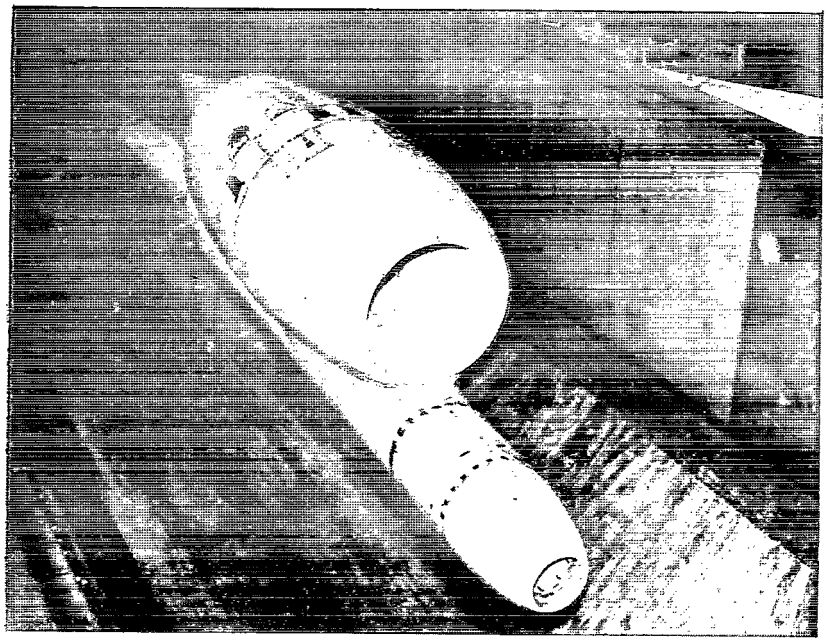

(a) Three-quarter front view. L-65-4786

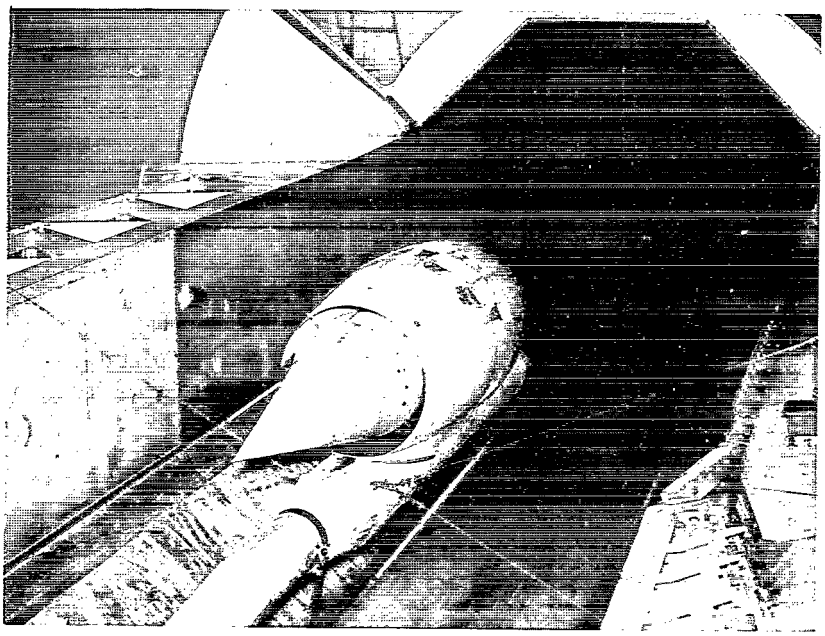

(b) Three-quarter rear view.

Figure 3.- Photographs of cruise fan. L-65-4788

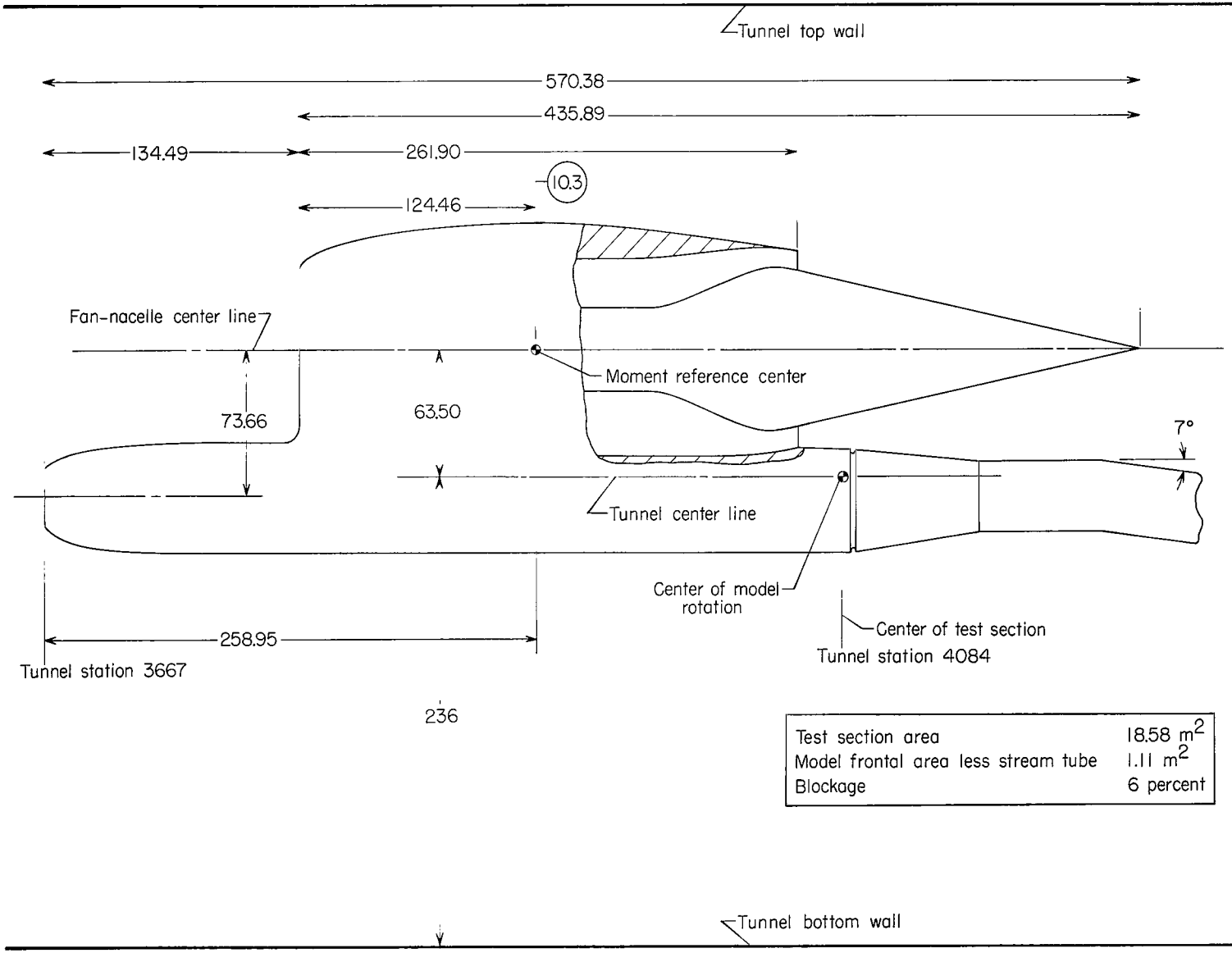

Figure 4.- Installation of cruise fan in the Langley 16-foot transonic tunnel. All dimensions are in centimeters unless otherwise noted.

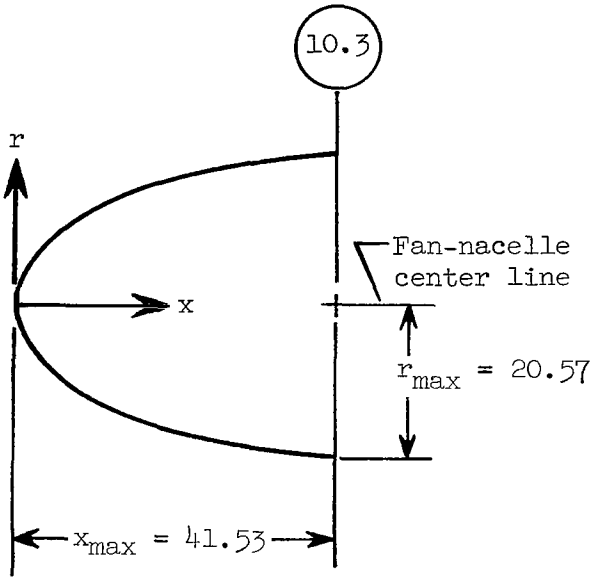

x/x_{max}	r/r_{max}
0.0	0.0
.028	.220
.056	.289
.085	.356
.141	.456
.281	.637
.470	.795
.705	.940
.893	.998
1.000	1.000

(a) Fan-bulletnose ordinates.

Figure 5.- Geometric characteristics of the various model components. All dimensions in centimeters unless otherwise noted.

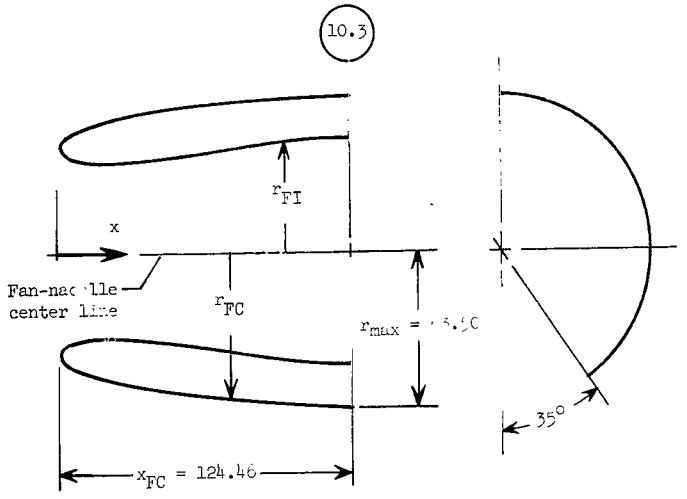

x/x_{FC}	r_{FI}/r_{max}	r_{FC}/r_{max}
0.0	0.649	0.649
.007		.680
.010	.615	
.015		.693
.020	.602	
.022		.703
.030	.594	.713
.060	.579	.744
.092		.768
.097	.573	
.150	.573	.809
.300	.584	.876
.500	.616	.942
.750	.694	.989
.933	.720	
.950		.998
1.000	.720	1.000

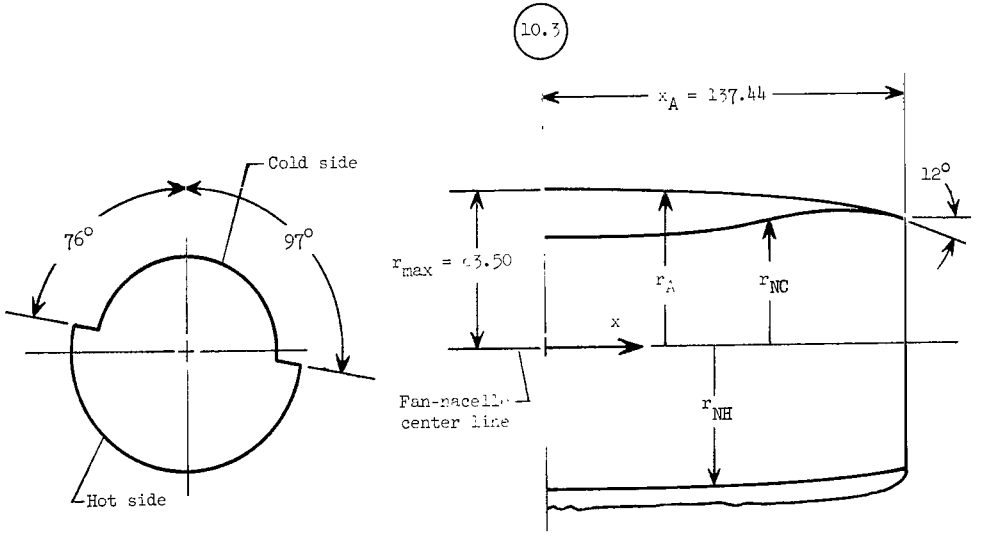

x/x_A	r_{NC}/r_{max}	r_{NH}/r_{max}	r_A/r_{max}
0.0	0.720	0.833	1.000
.111			.977
.185	.720	.833	
.221			.988
.388			.965
.397	.720	.833	
.506	.749	.833	
.554			.930
.617	.782	.833	
.710	.782	.833	
.775			.863
.801	.782	.833	
.843	.829	.829	.838
.889	.818	.818	
.935	.798	.798	
.951	.777	.777	.779
1.000	.768	.768	.772

(b) Fan-inlet, cowl, nozzle-shroud, and afterbody ordinates. (Note: r_{FC}/r_{max} and r_A/r_{max} ordinates are applicable ±145° from vertical, for other ±35° see fig. 5(c).)

Figure 5.- Continued.

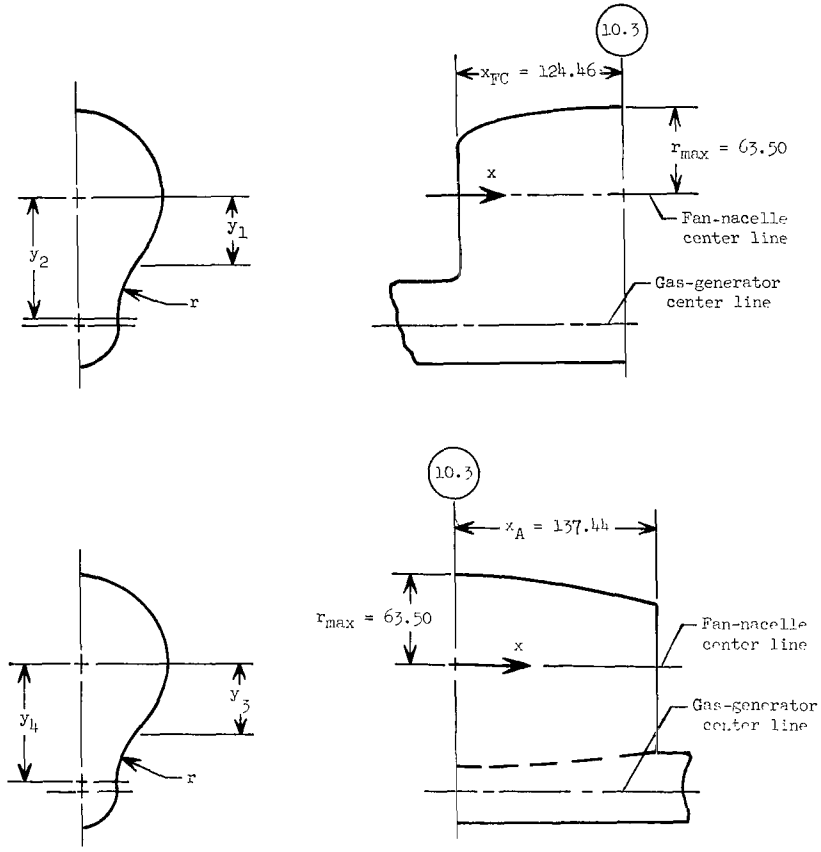

x/x_{FC}	y_1/x_{FC}	y_2/x_{FC}	r/r_{max}
0.0	0.331	0.367	0.072
.030	.308	.401	.106
.060	.331	.417	.108
.090	.341	.430	.108
.150	.349	.439	.112
.300	.360	.459	.132
.500	.370	.500	.191
.750	.396	.543	.316
.950	.418	.571	.328
1.000	.421	.573	.340

x/x_A	y_3/x_A	y_4/x_A	r/r_{max}
0.0	0.382	0.519	.340
.111	.378	.517	.332
.222	.374	.516	.328
.388	.365	.495	.280
.554	.362	.481	.240
.775	.359	.420	.100
.843	.358	.390	.044
1.000	.357	.357	0.0

(c) Fan cowl and afterbody to gas-generator-nacelle fairing ordinates. (Note: Radii of fairing intersects gas-generator nacelle with fan cowl or afterbody at points y_1, y_2, y_3, or y_4.)

Figure 5.- Continued.

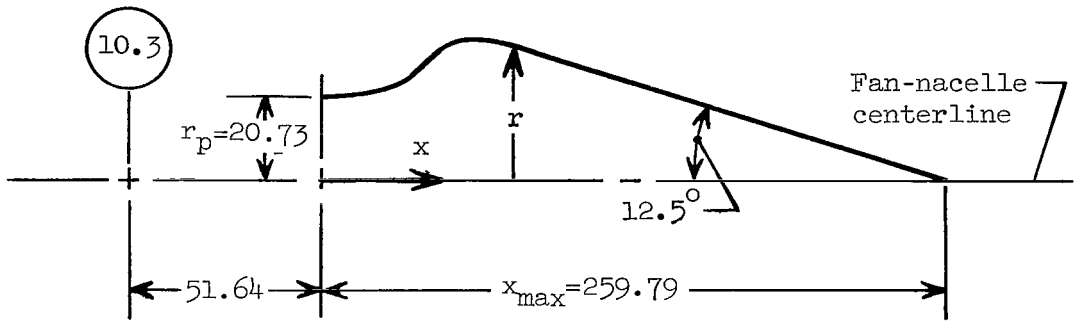

x/x_{max}	r/r_p
0.0	1.000
.060	1.188
.120	1.455
.180	1.726
.240	1.954
.300	1.923
.310	1.901
.320	1.875
.330	1.846
.340	1.825
.350	1.798
.360	1.770
.480	1.440
.600	1.106
.720	.773
.840	.416
1.000	0.0

(d) Plug ordinates.

Figure 5.- Continued.

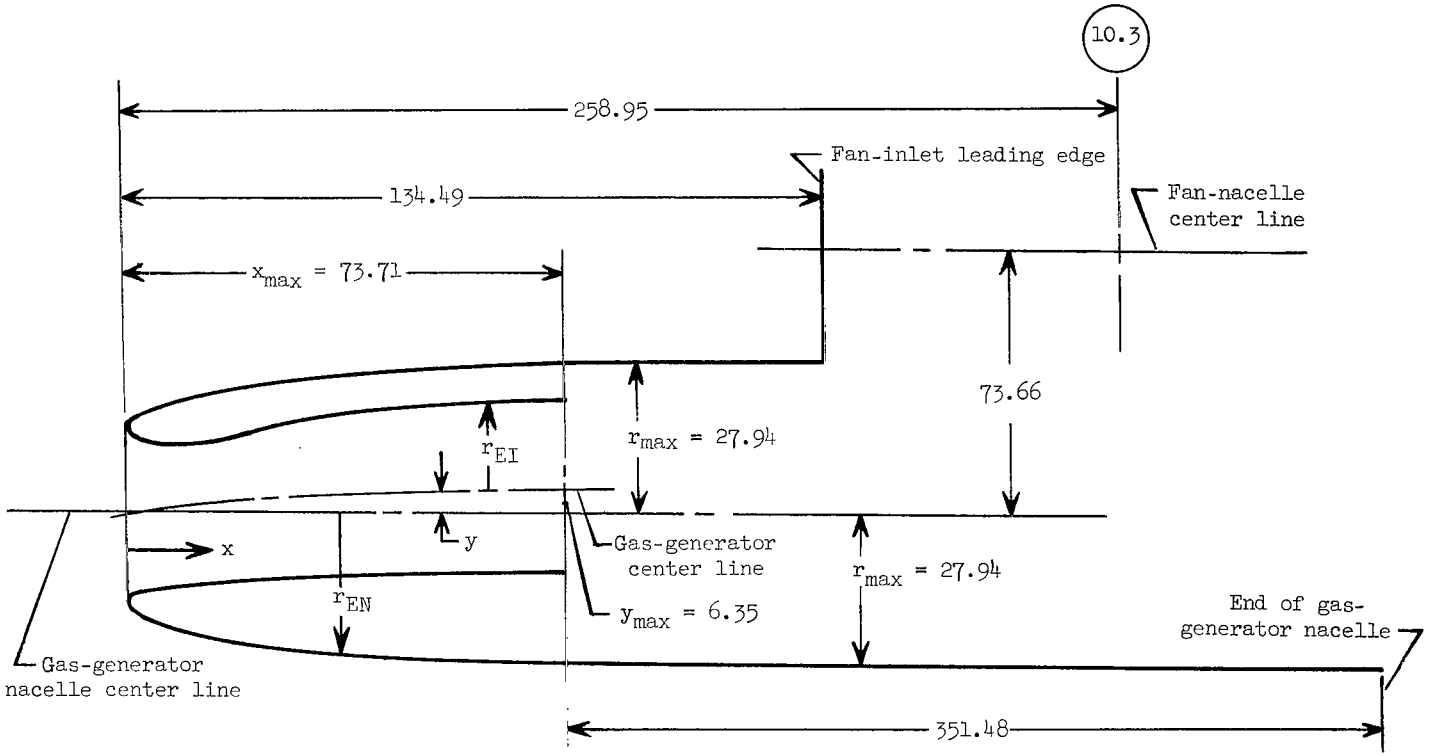

x/x_{max}	y/y_{max}	r_{EI}/r_{max}
0.0	0.0	0.512
.014	0.0	.471
.027	0.0	.456
.043	0.0	.452
.082	.030	.450
.166	.150	.454
.330	.350	.465
.661	.850	.486
1.000	1.000	.487

x/x_{max}	r_{EN}/r_{max}
0.0	0.512
.041	.632
.083	.689
.166	.771
.331	.876
.661	.989
1.000	1.000

(e) Gas-generator-inlet and nacelle ordinates.

Figure 5.- Continued.

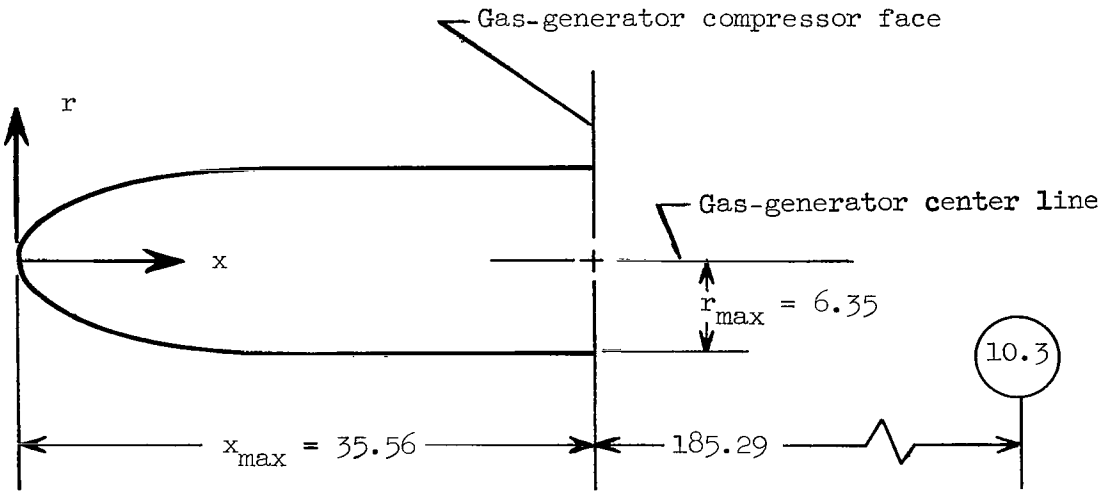

x/x_{max}	r/r_{max}
0.0	0.0
.071	.600
.143	.800
.214	.920
.357	1.000
1.000	1.000

(f) Gas-generator-bulletnose ordinates.

Figure 5.- Concluded.

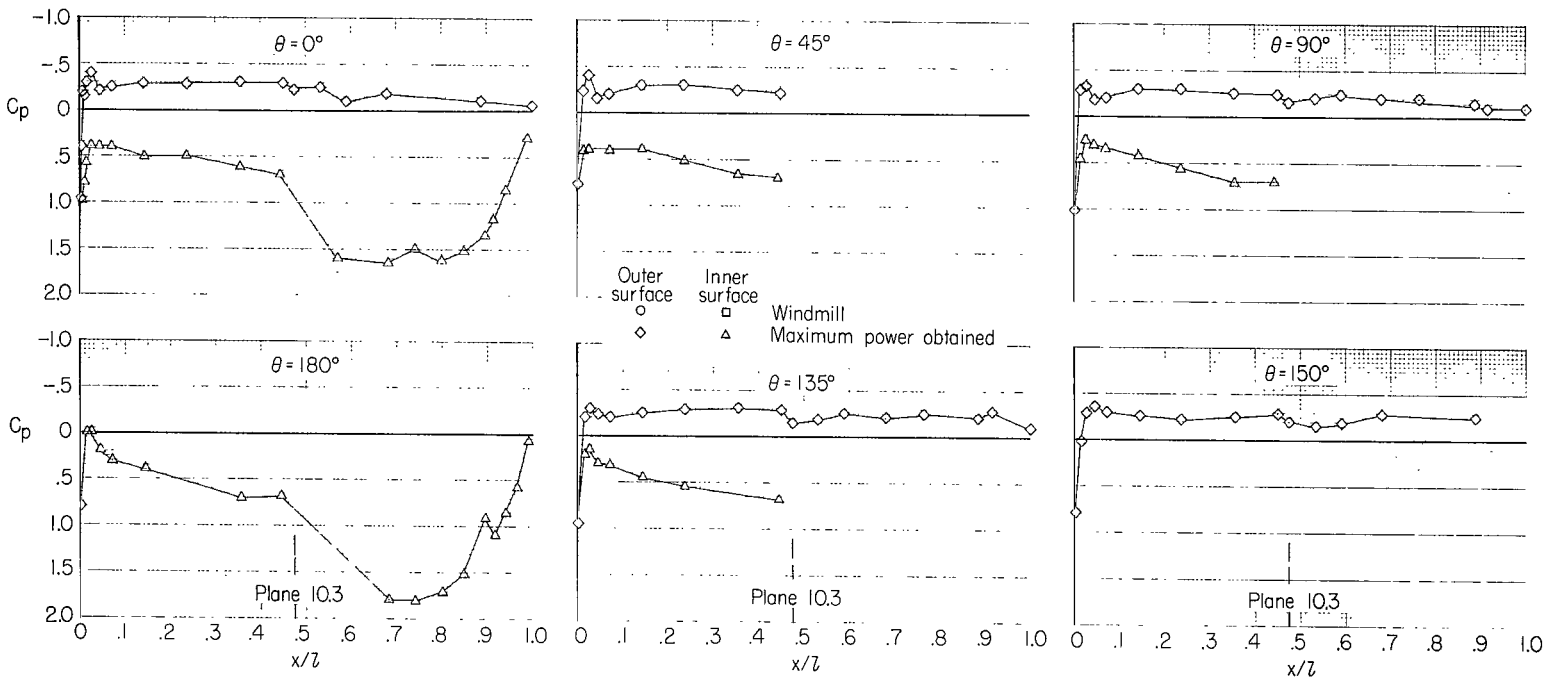

(a) $\alpha = -2^0$.

Figure 6.- Fan-nacelle-afterbody pressure distributions at M = 0.30 at various angles of attack.

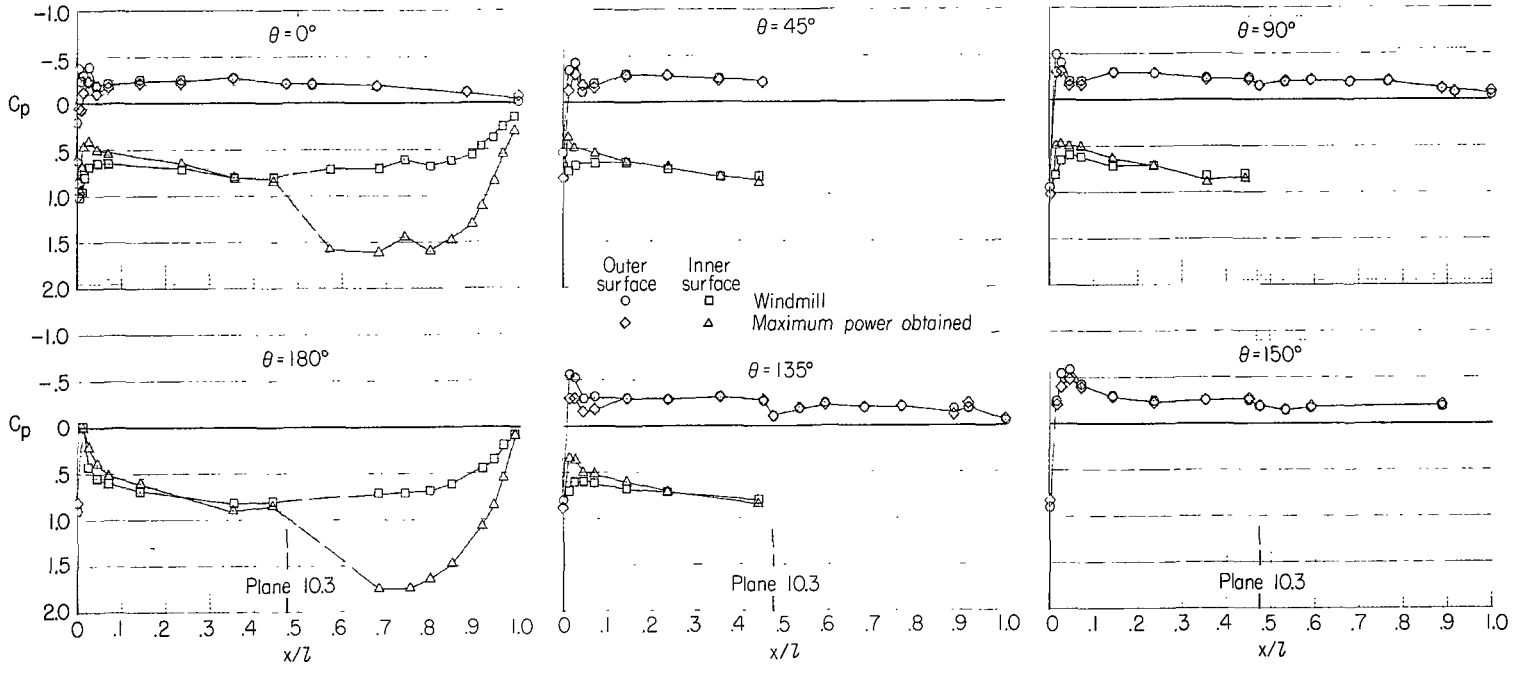

(b) $\alpha = 0^0$.

Figure 6.- Continued.

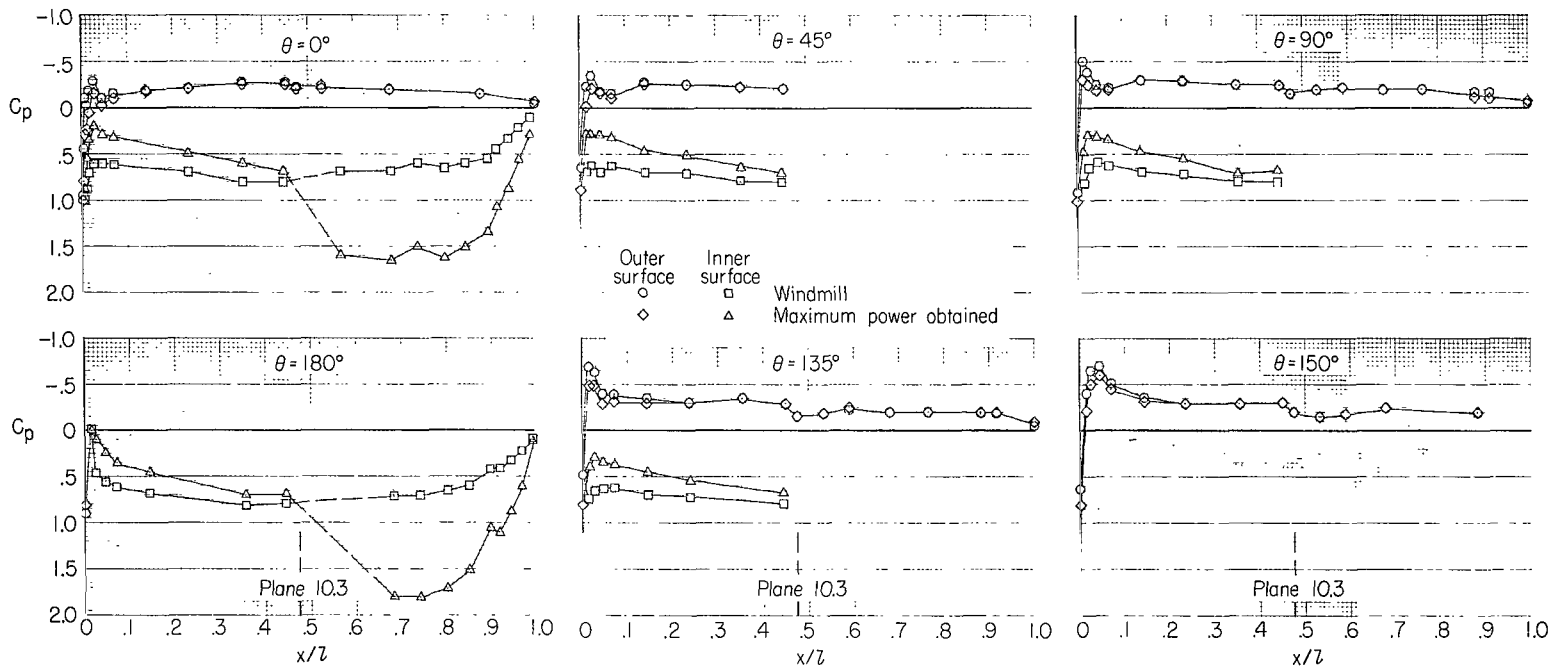

(c) $\alpha = 2^0$.

Figure 6.- Continued.

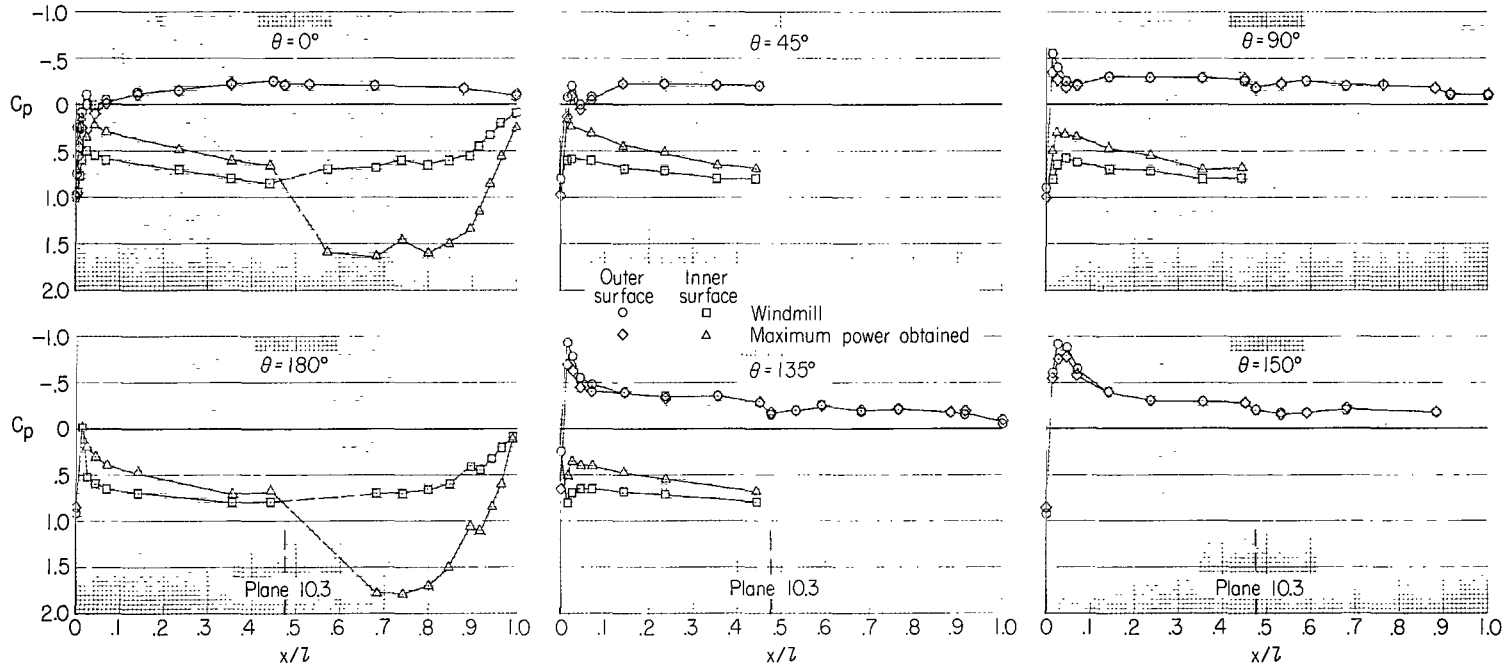

(d) $\alpha = 5^0$.

Figure 6.- Continued.

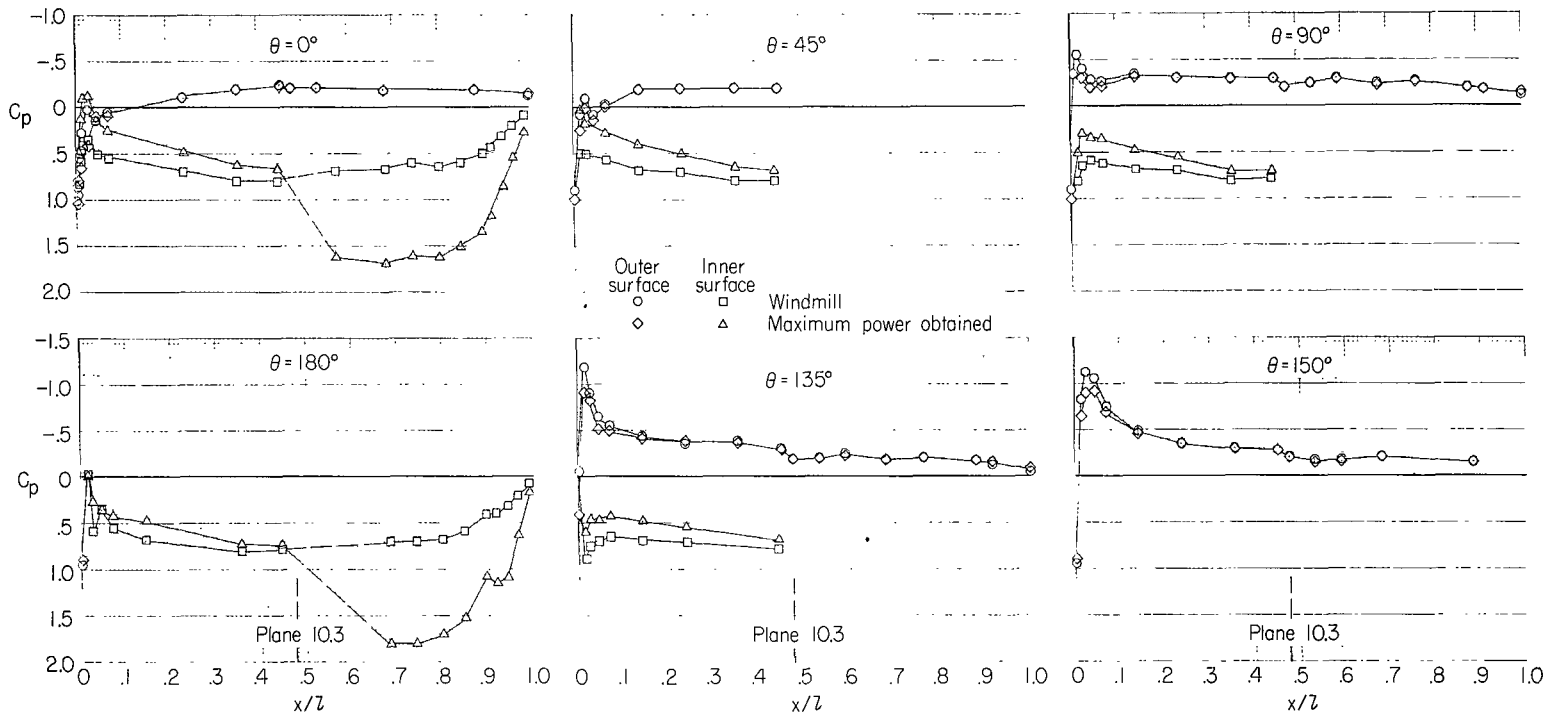

(e) $\alpha = 8^0$.

Figure 6.- Concluded.

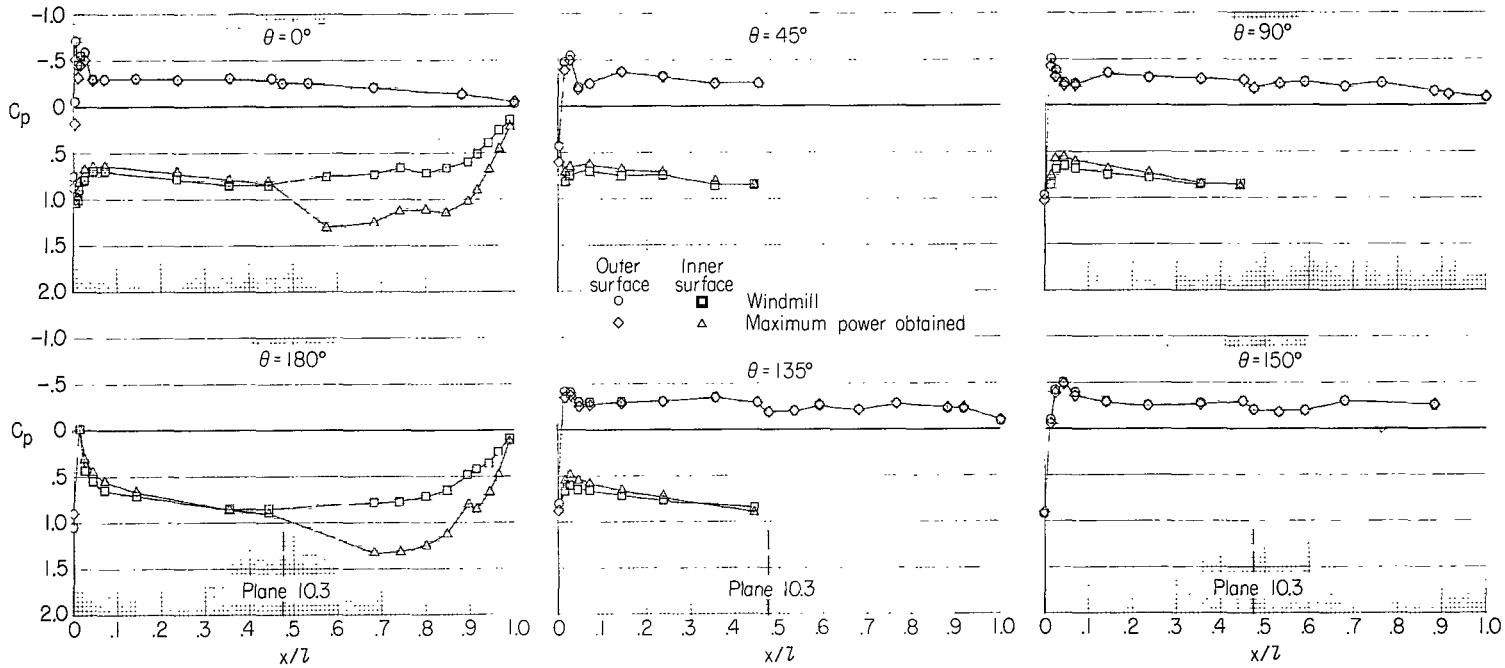

(a) $\alpha = -2^0$.

Figure 7.- Fan-nacelle-afterbody pressure distributions at M = 0.50 at various angles of attack.

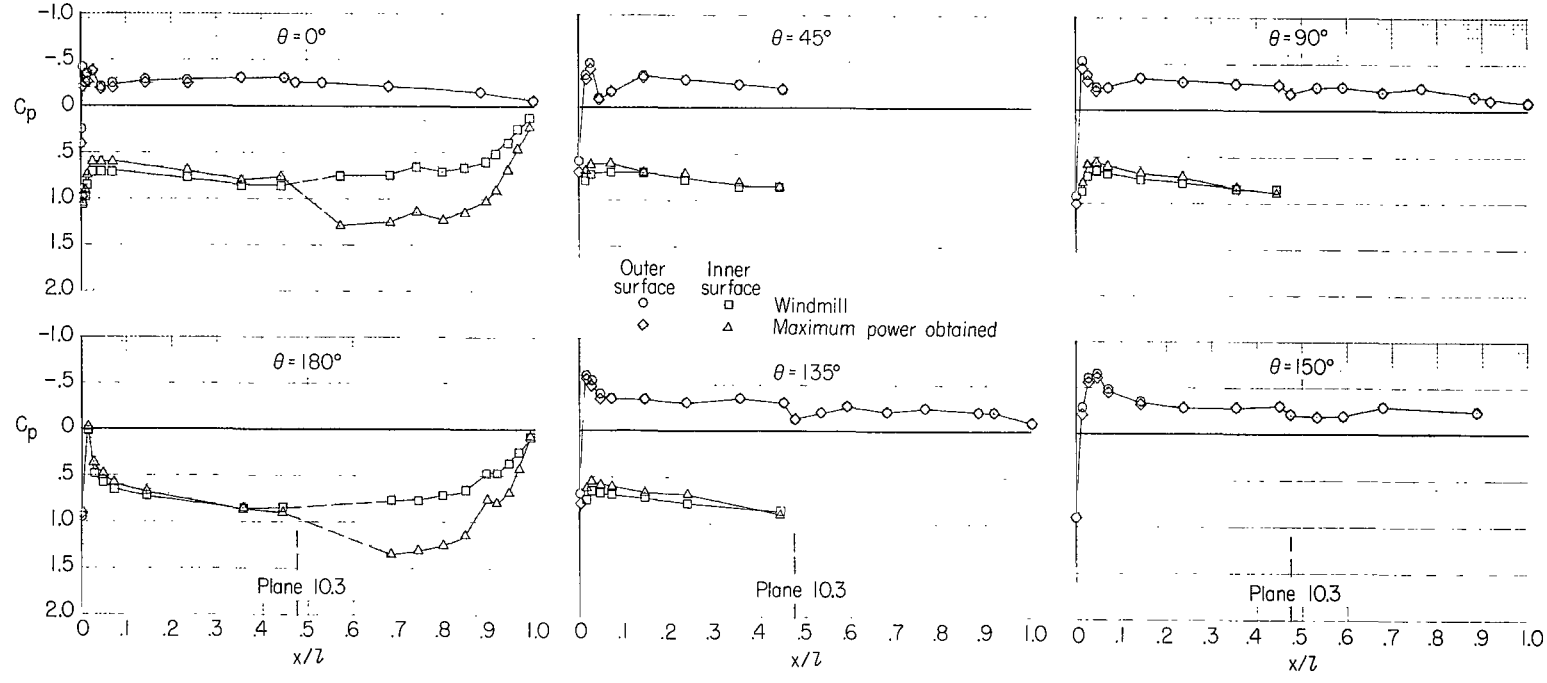

(b) $\alpha = 0^0$.

Figure 7.- Continued.

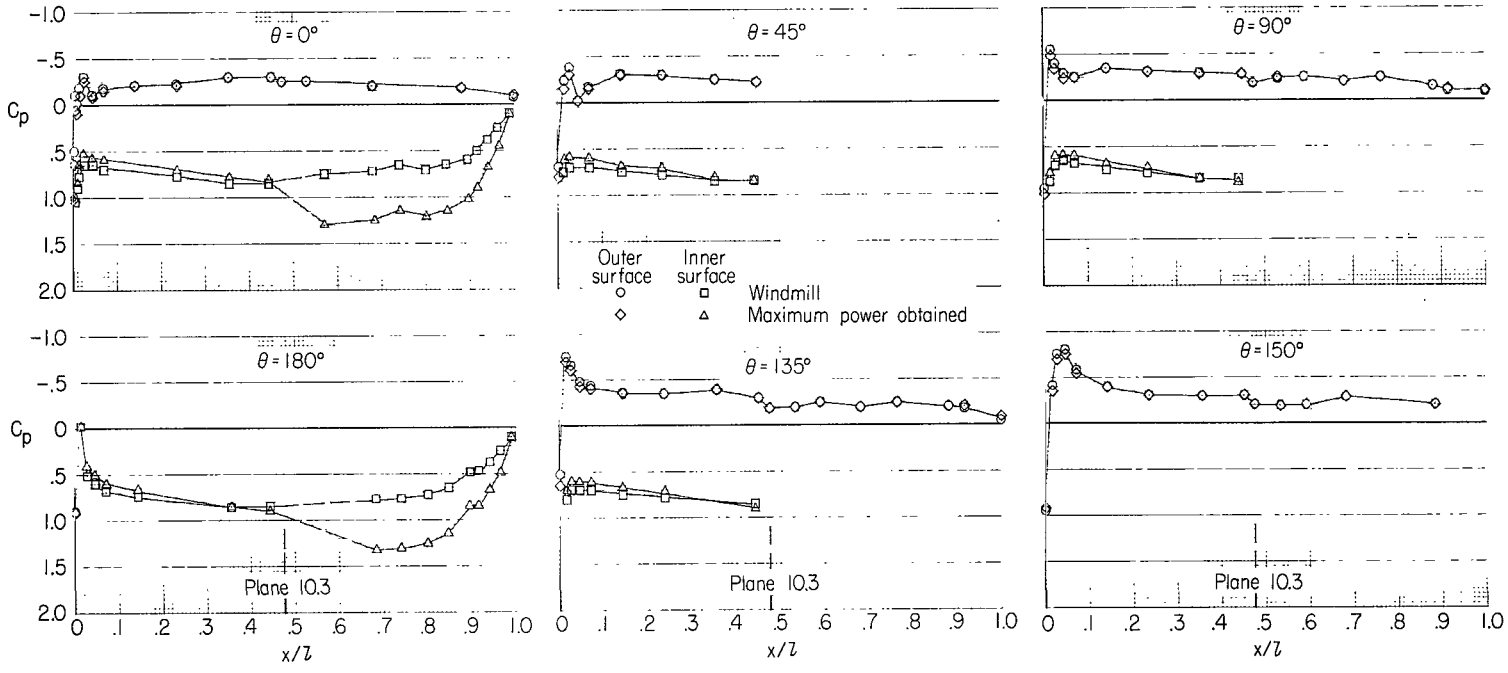

(c) $\alpha = 2^0$.

Figure 7.- Continued.

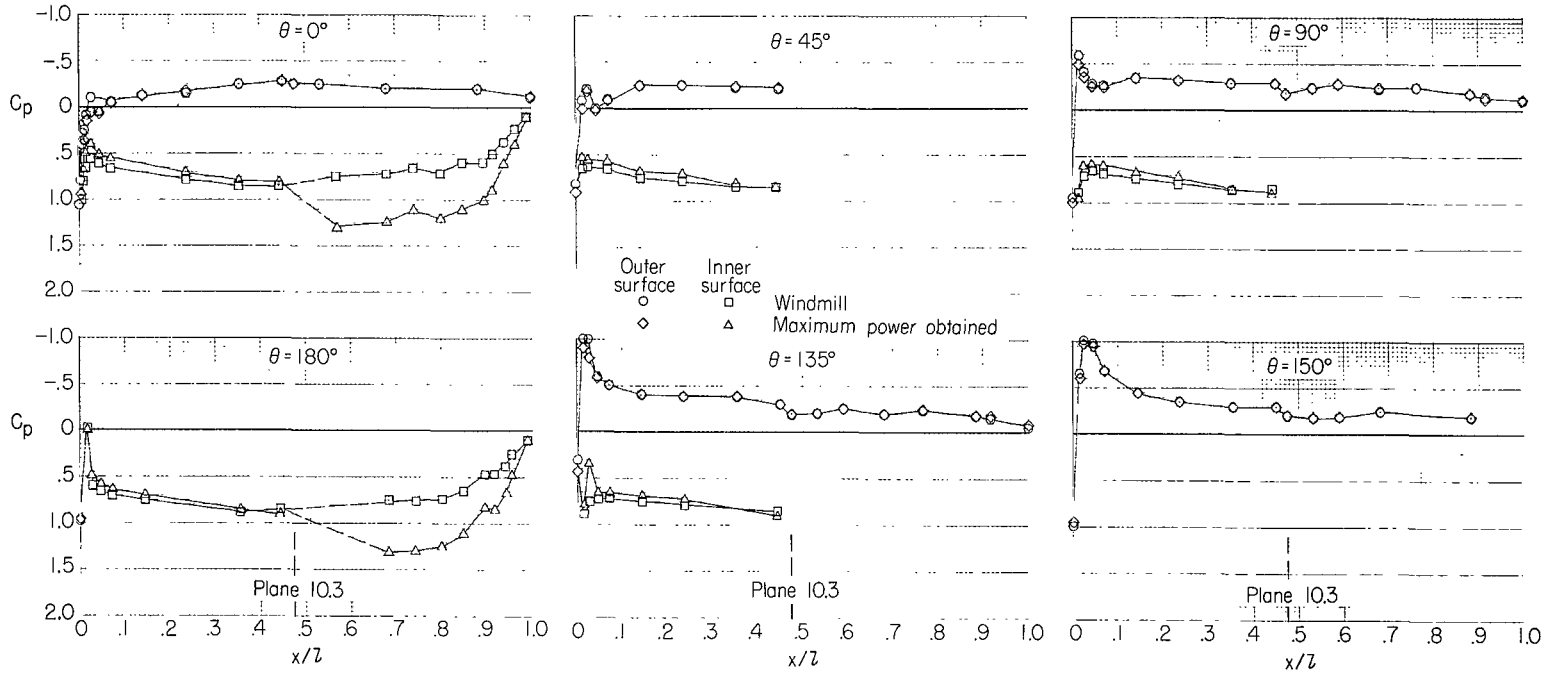

(d) $\alpha = 5^{0}$.

Figure 7.- Continued.

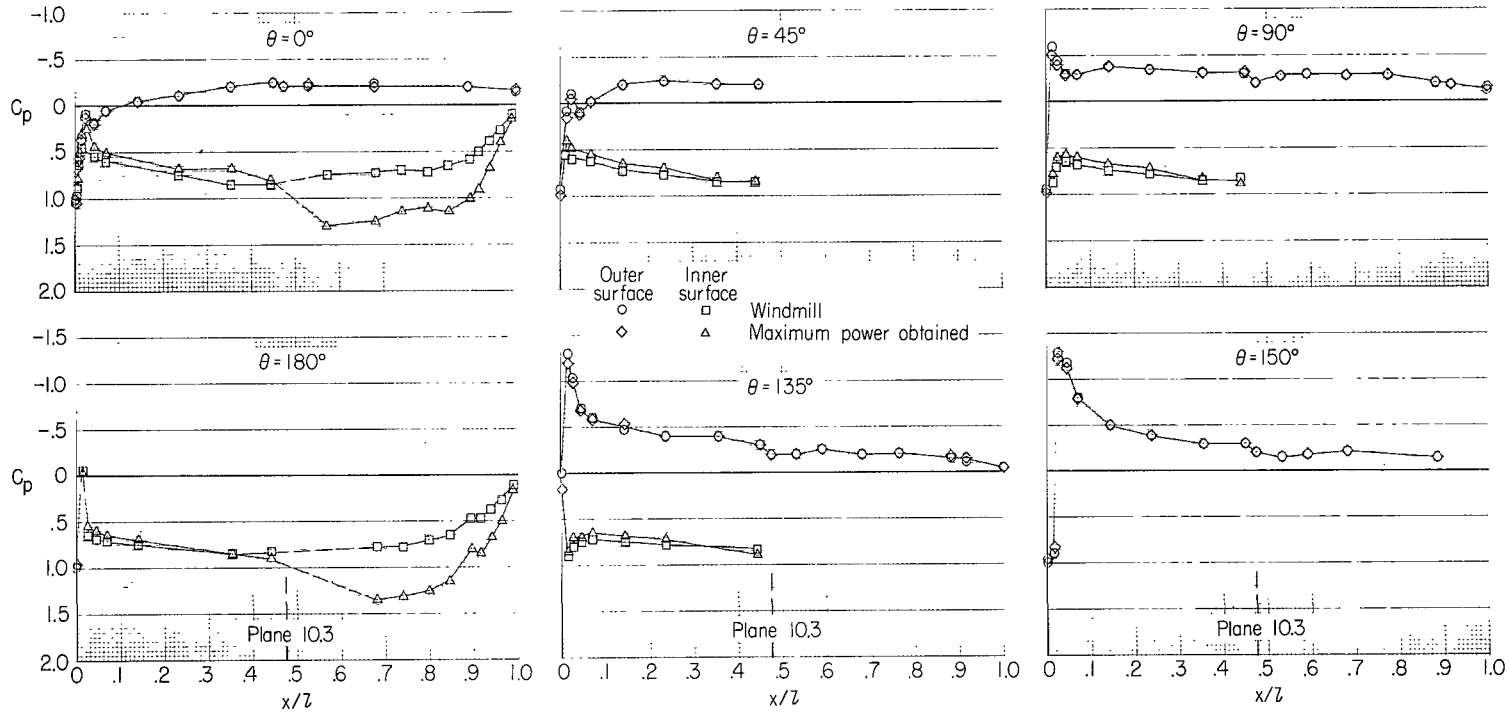

(e) $\alpha = 8^0$.

Figure 7.- Concluded.

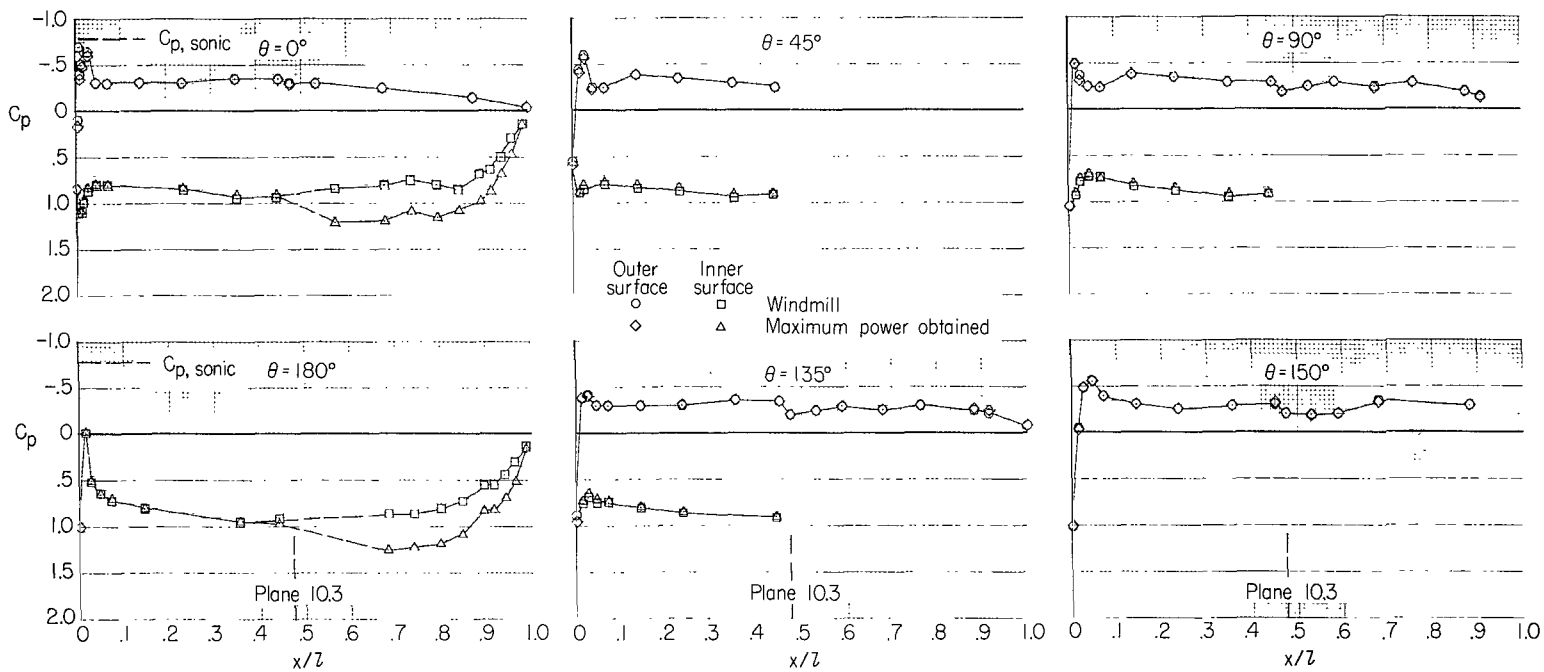

(a) $\alpha = -2^0$.

Figure 8.- Fan-nacelle-afterbody pressure distributions at M = 0.70 at various angles of attack.

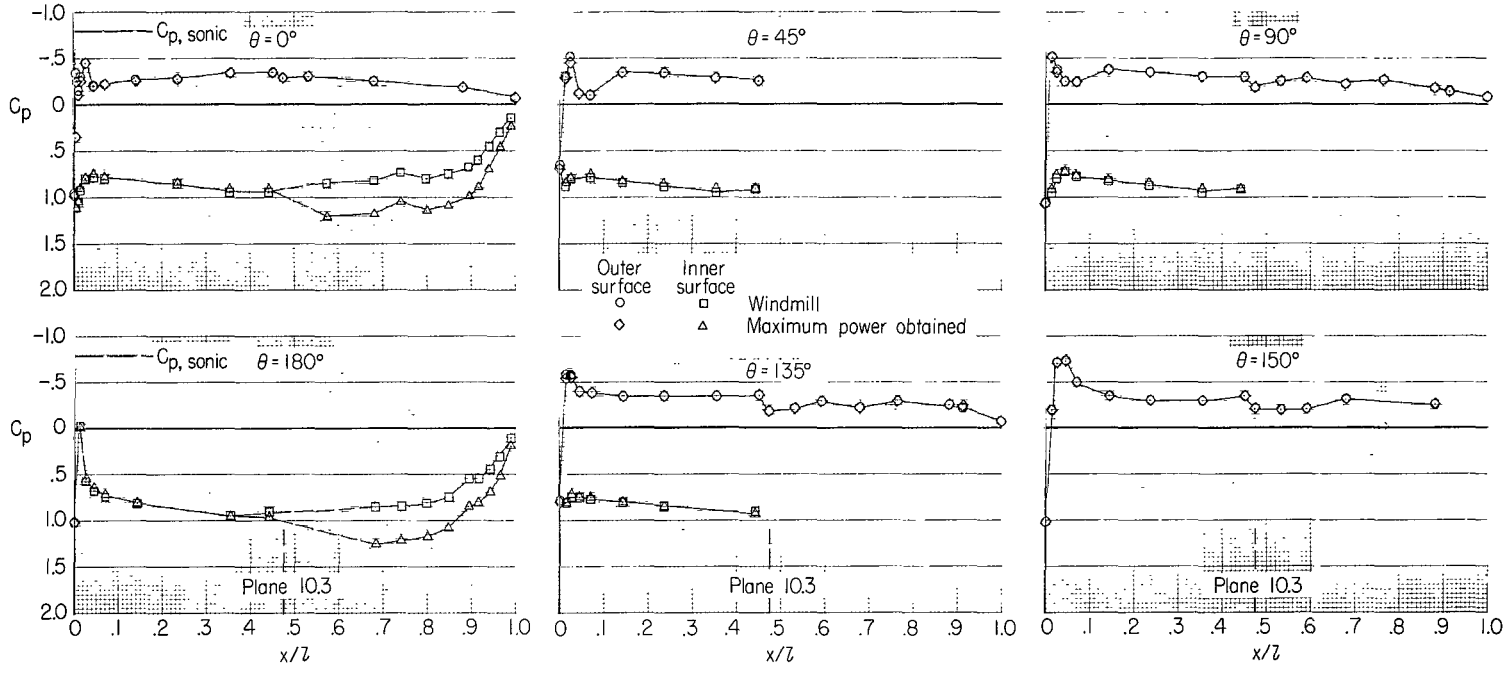

(b) $\alpha = 0^0$.

Figure 8.- Continued.

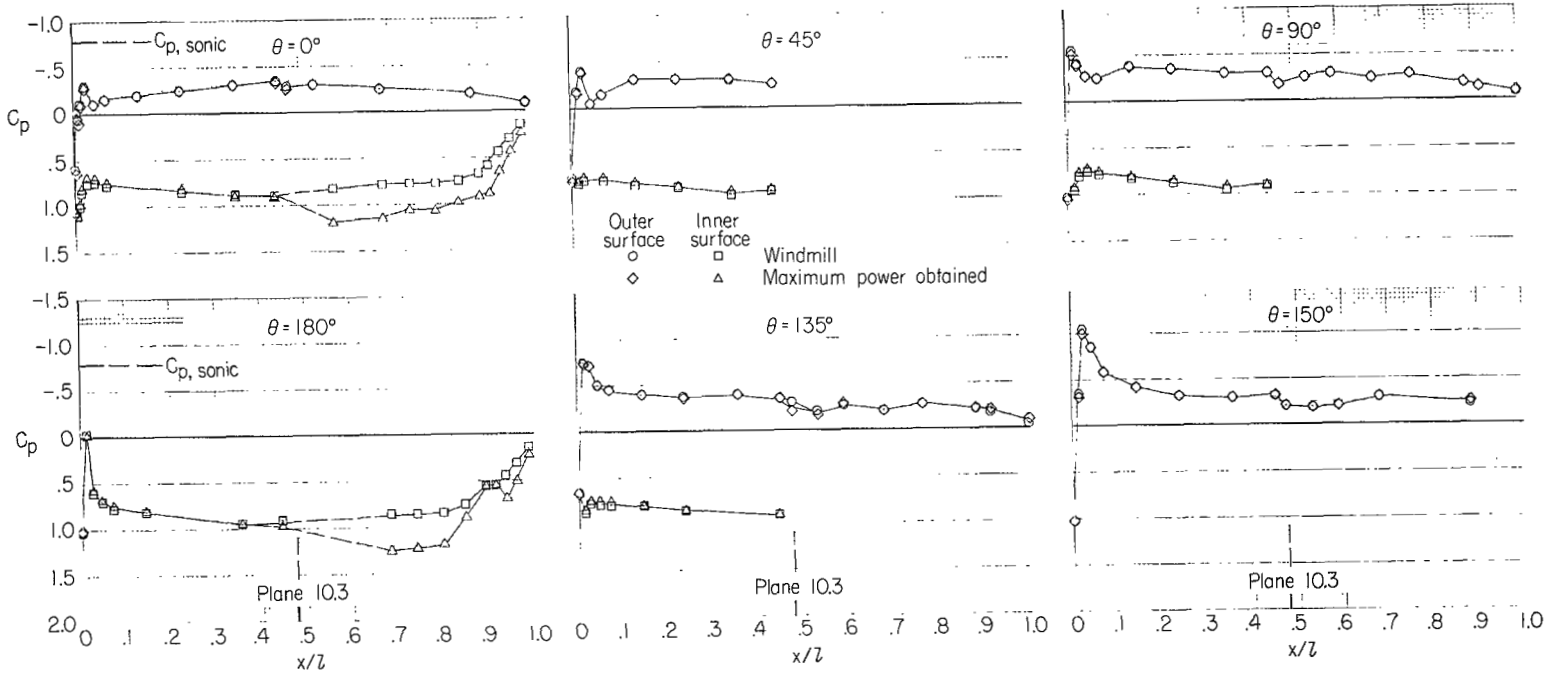

(c) $\alpha = 2^0$.

Figure 8.- Continued.

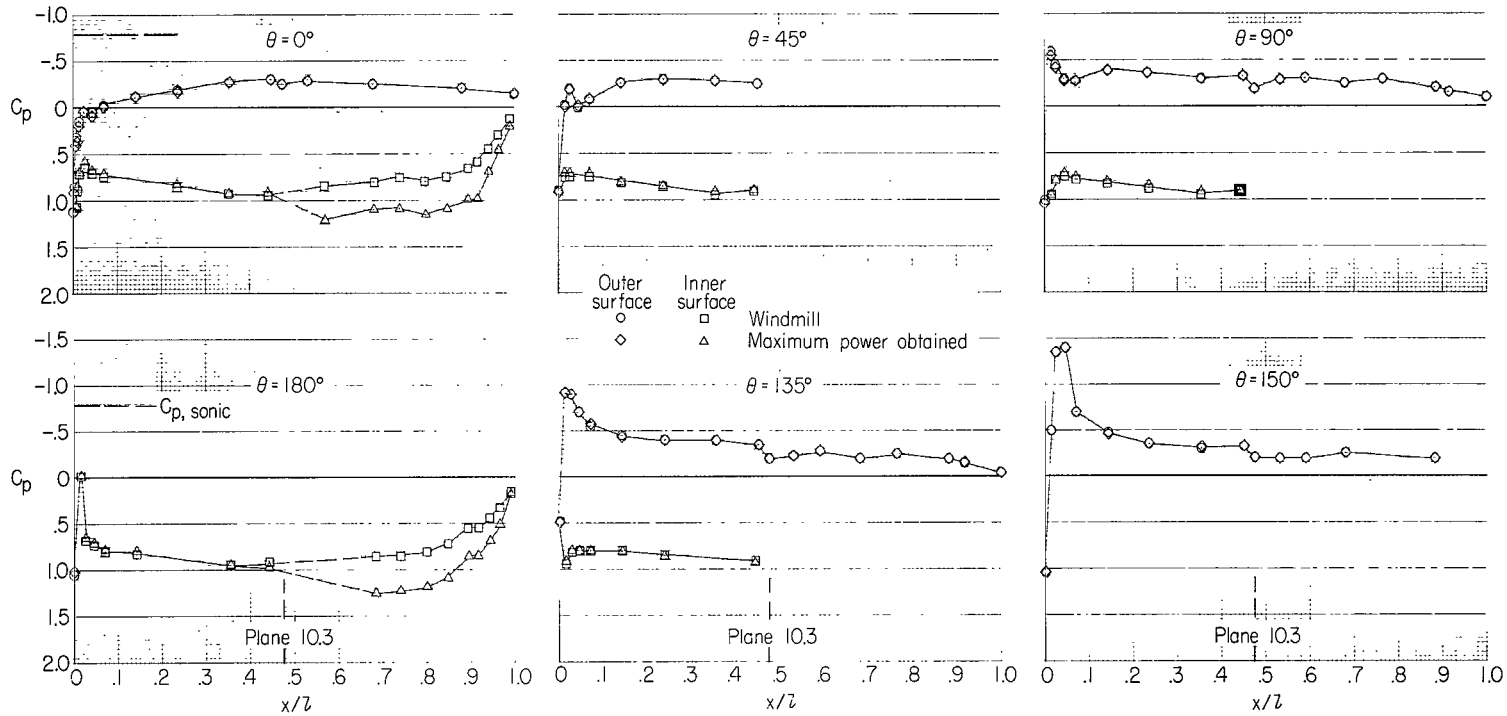

(d) $\alpha = 5^0$.

Figure 8.- Concluded.

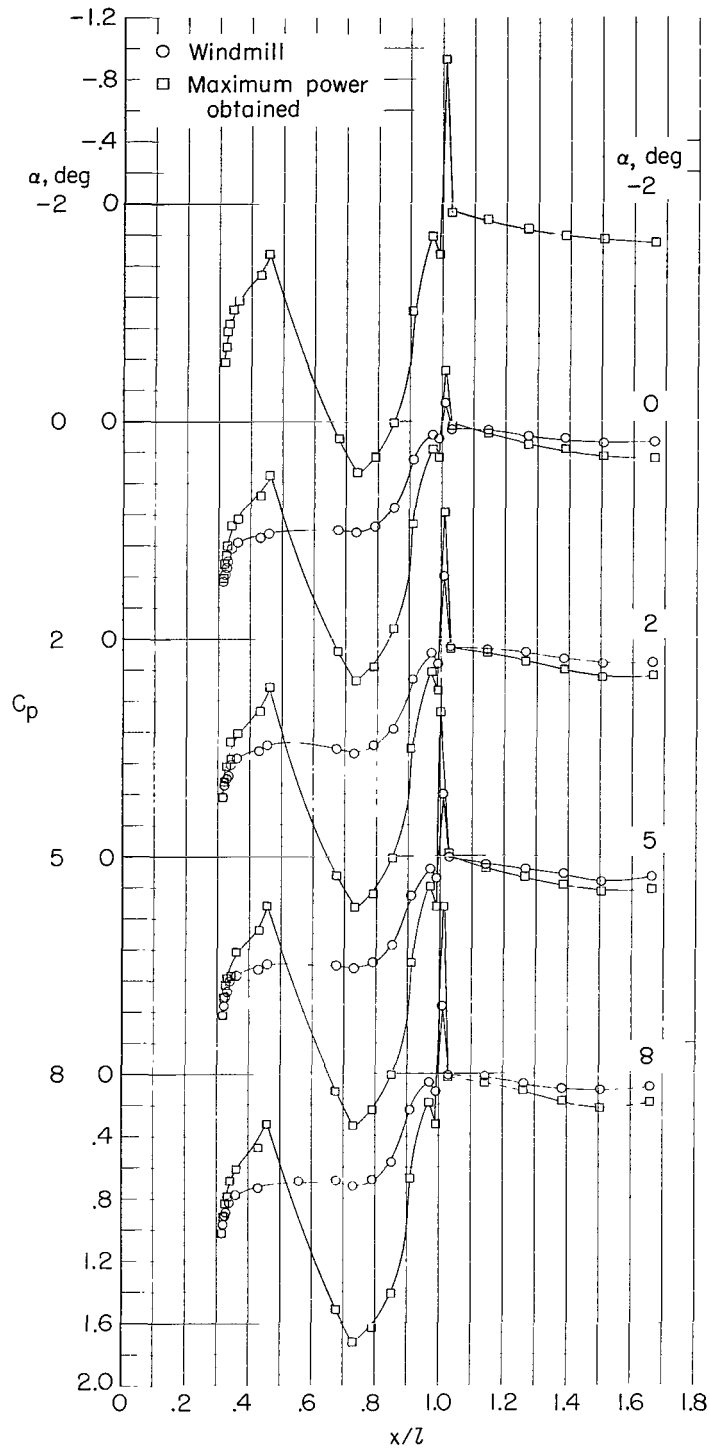

(a) $\theta = 0^0$.

Figure 9.- Fan-bulletnose-plus-plug pressure distributions at M = 0.30.

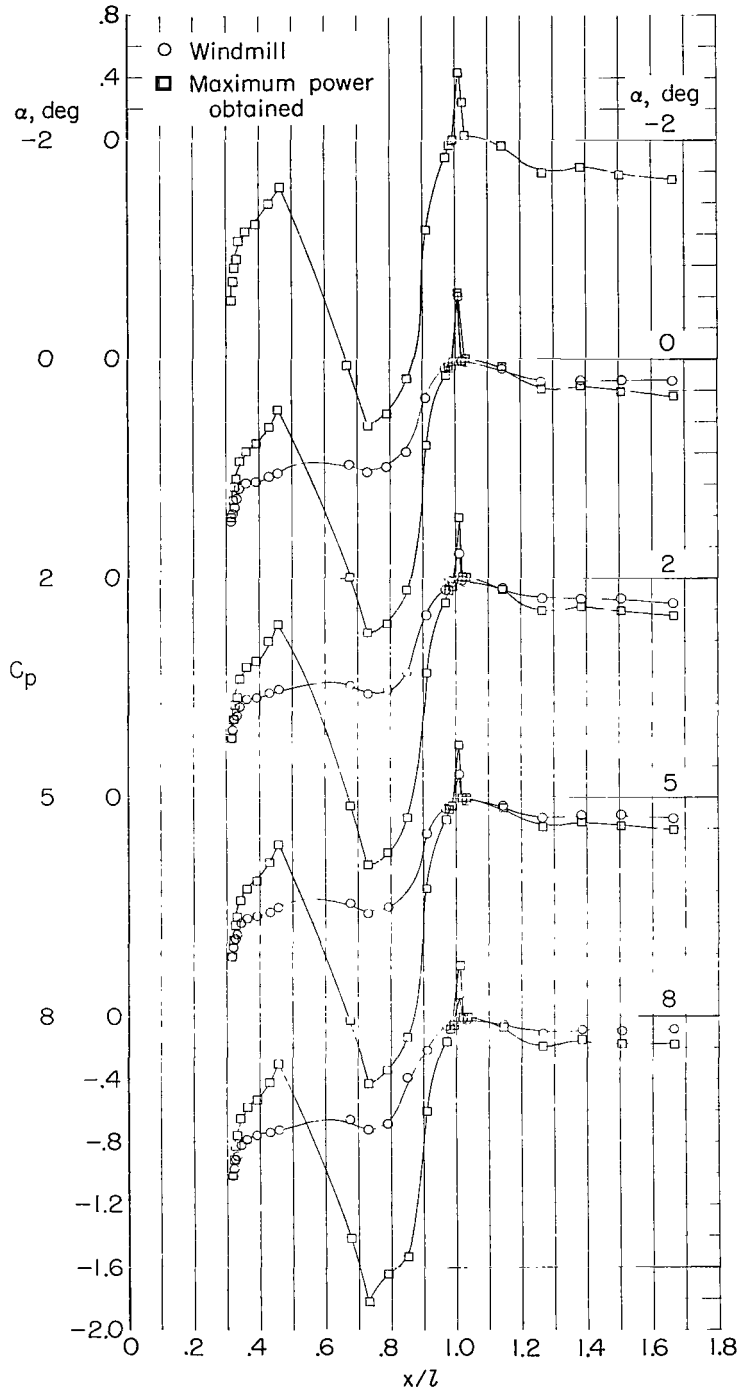

(b) $\theta = 180^0$.

Figure 9.- Concluded.

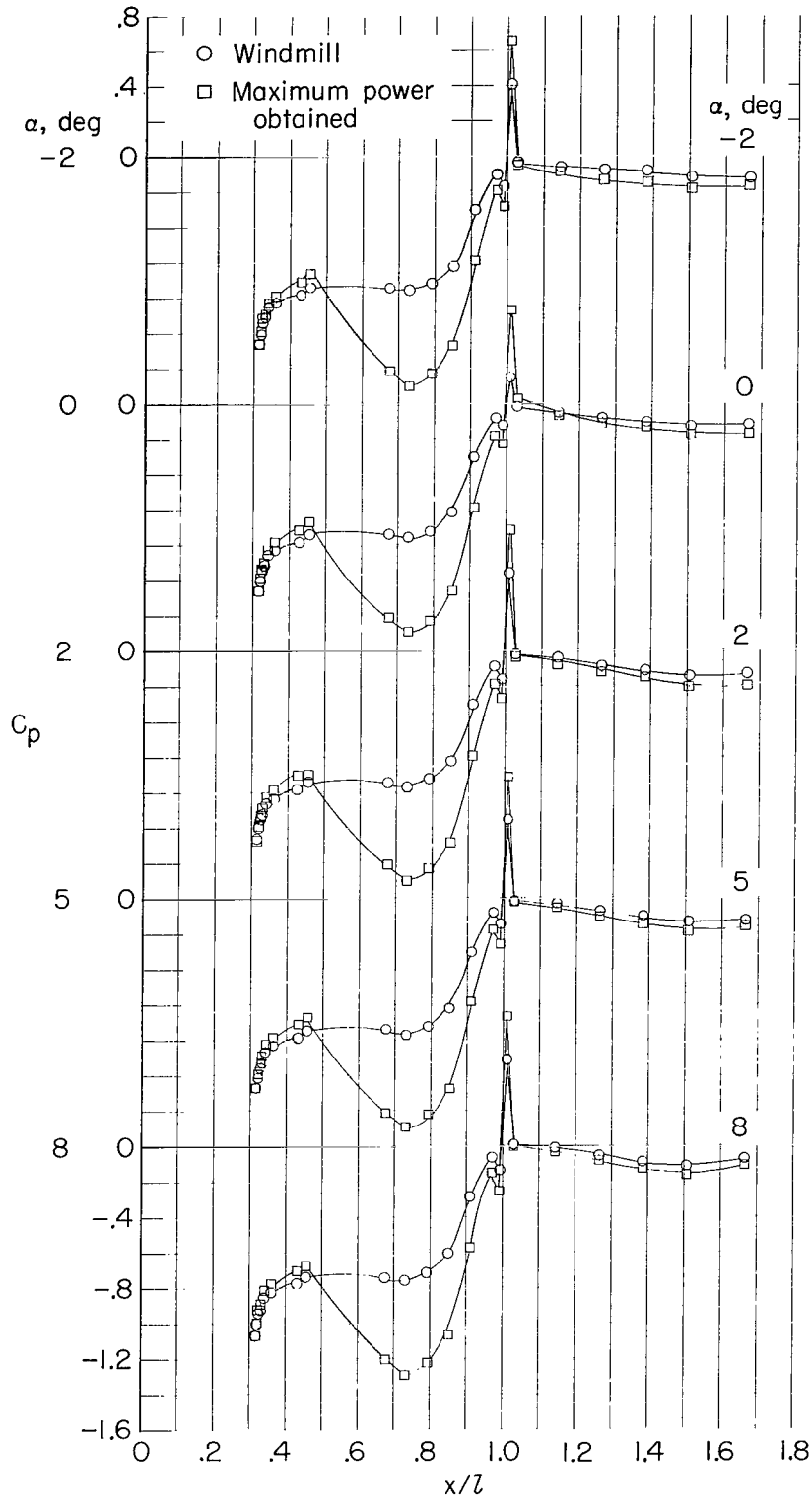

(a) $\theta = 0^0$.

Figure 10.- Fan-bulletnose-plus-plug pressure distributions at M = 0.50.

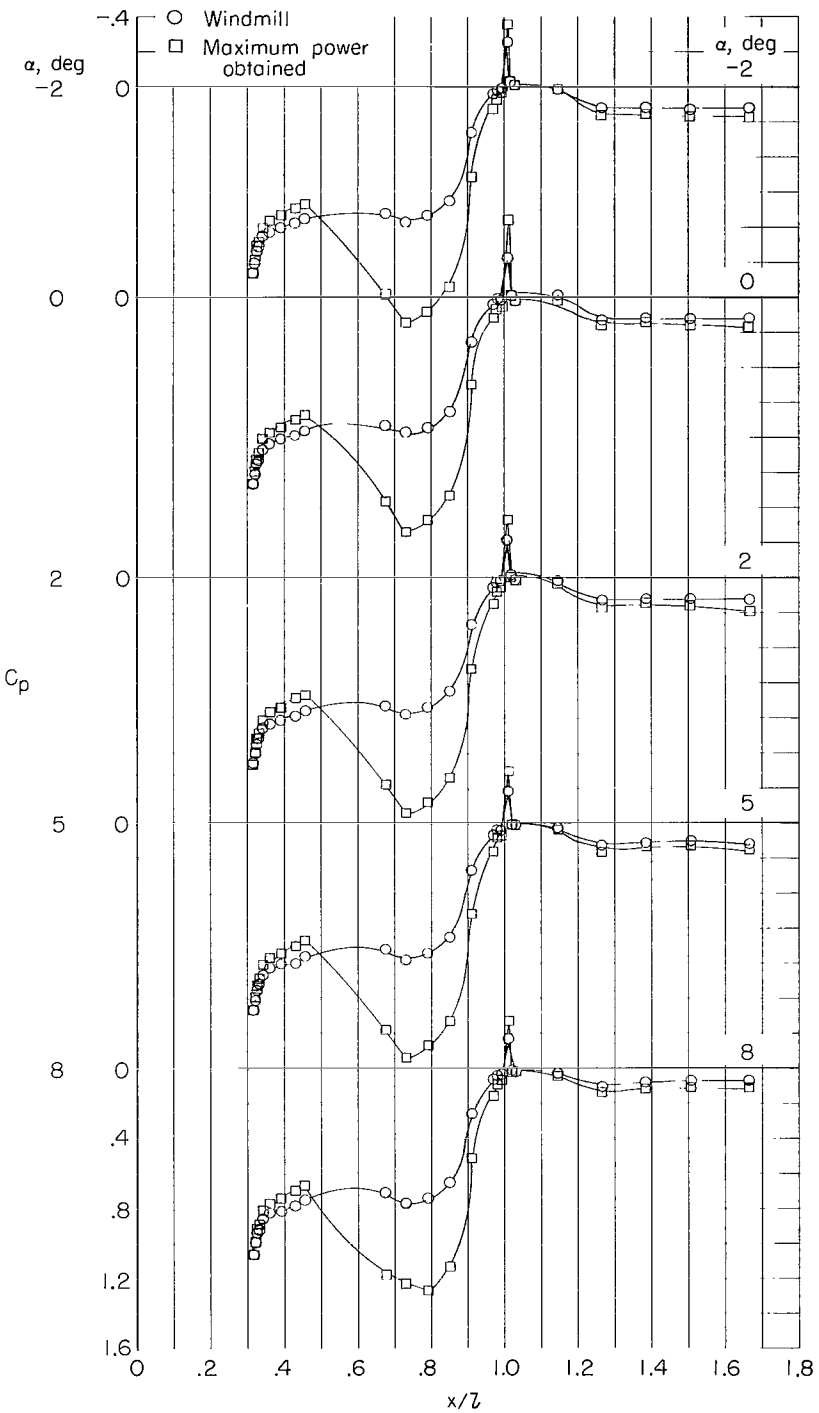

(b) $\theta = 180^0$.

Figure 10.- Concluded.

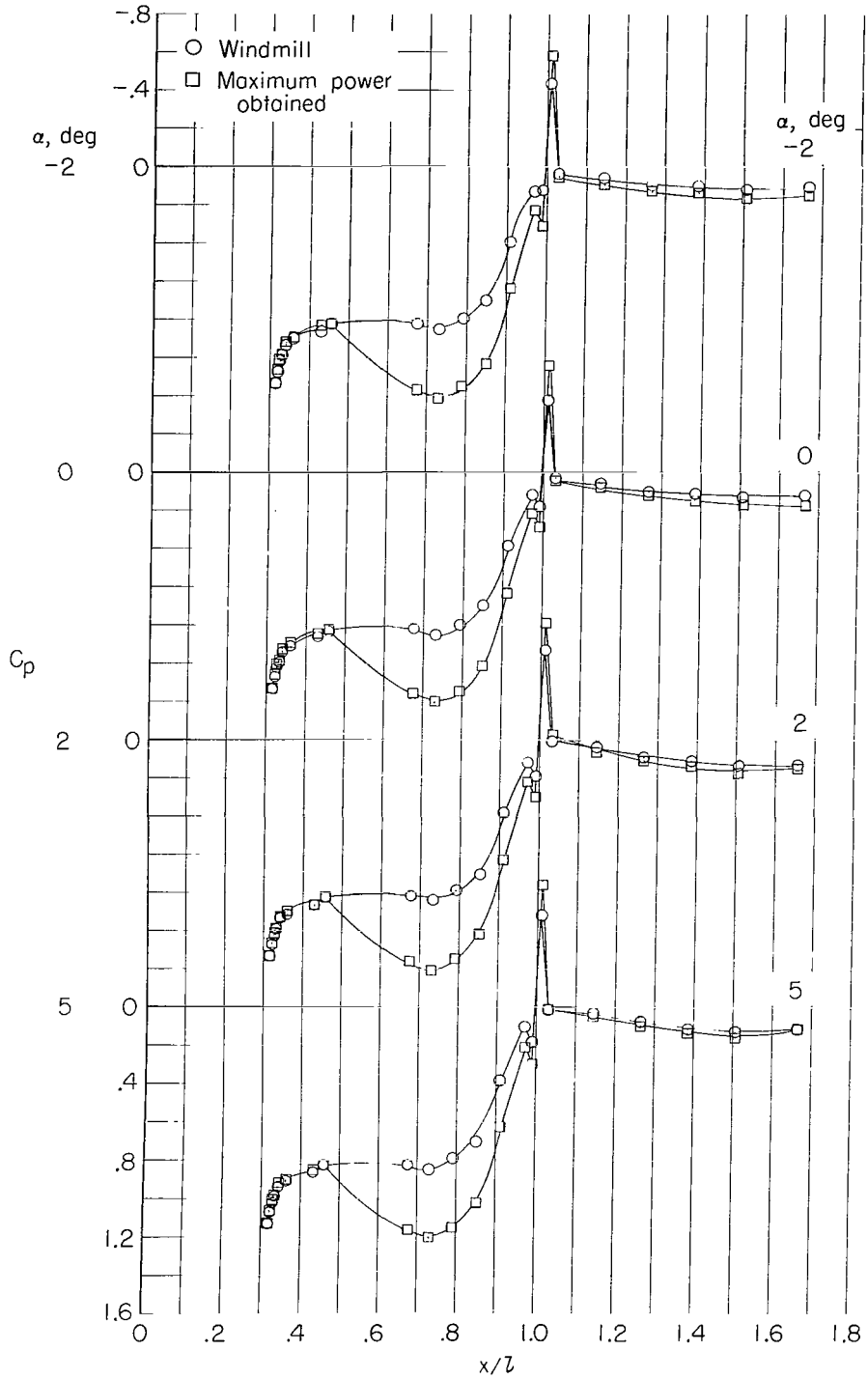

(a) $\theta = 0^0$.

Figure 11.- Fan-bulletnose-plus-plug pressure distributions at M = 0.70.

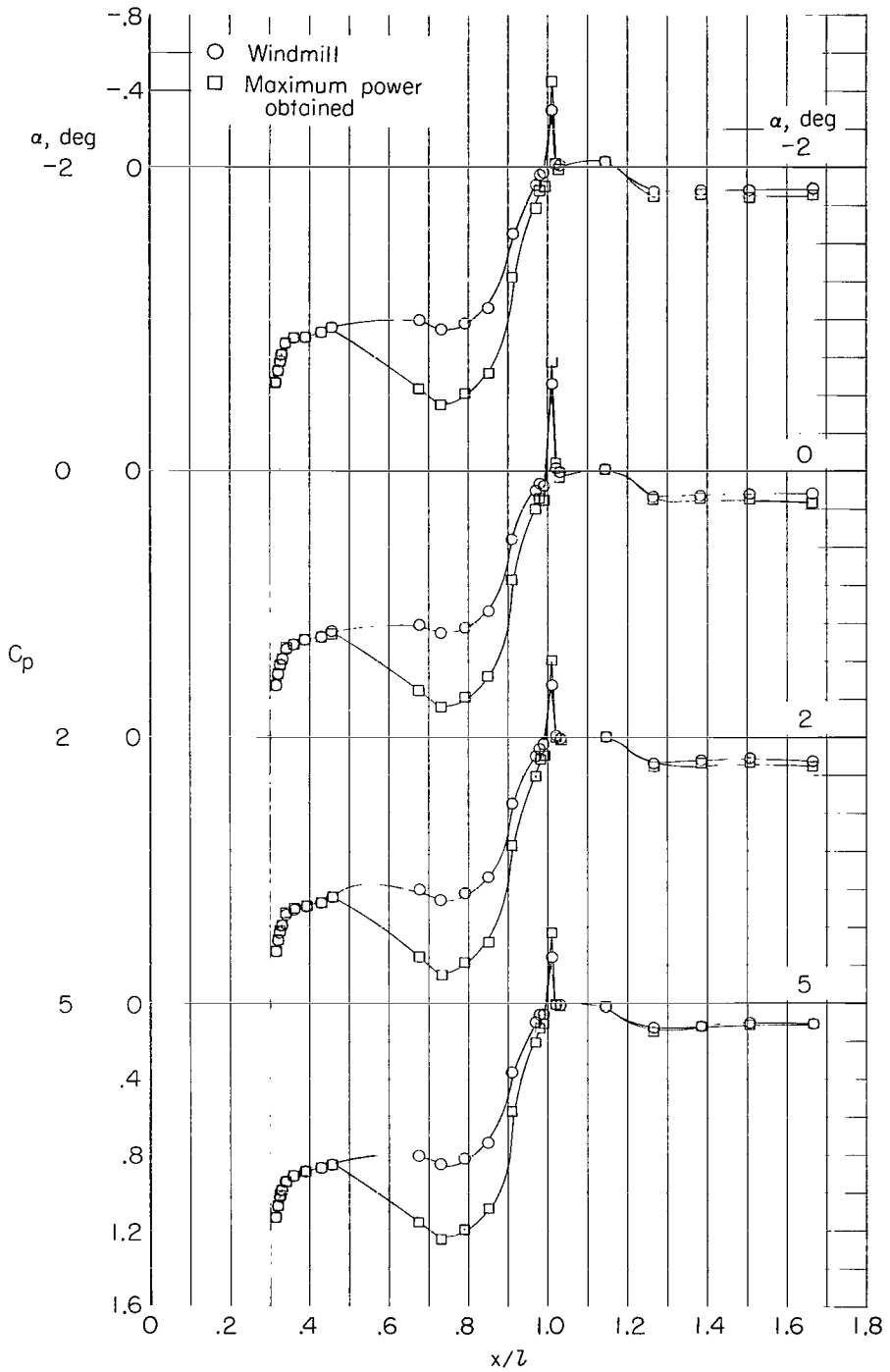

(b) $\theta = 180^{o}$.

Figure 11.- Concluded.

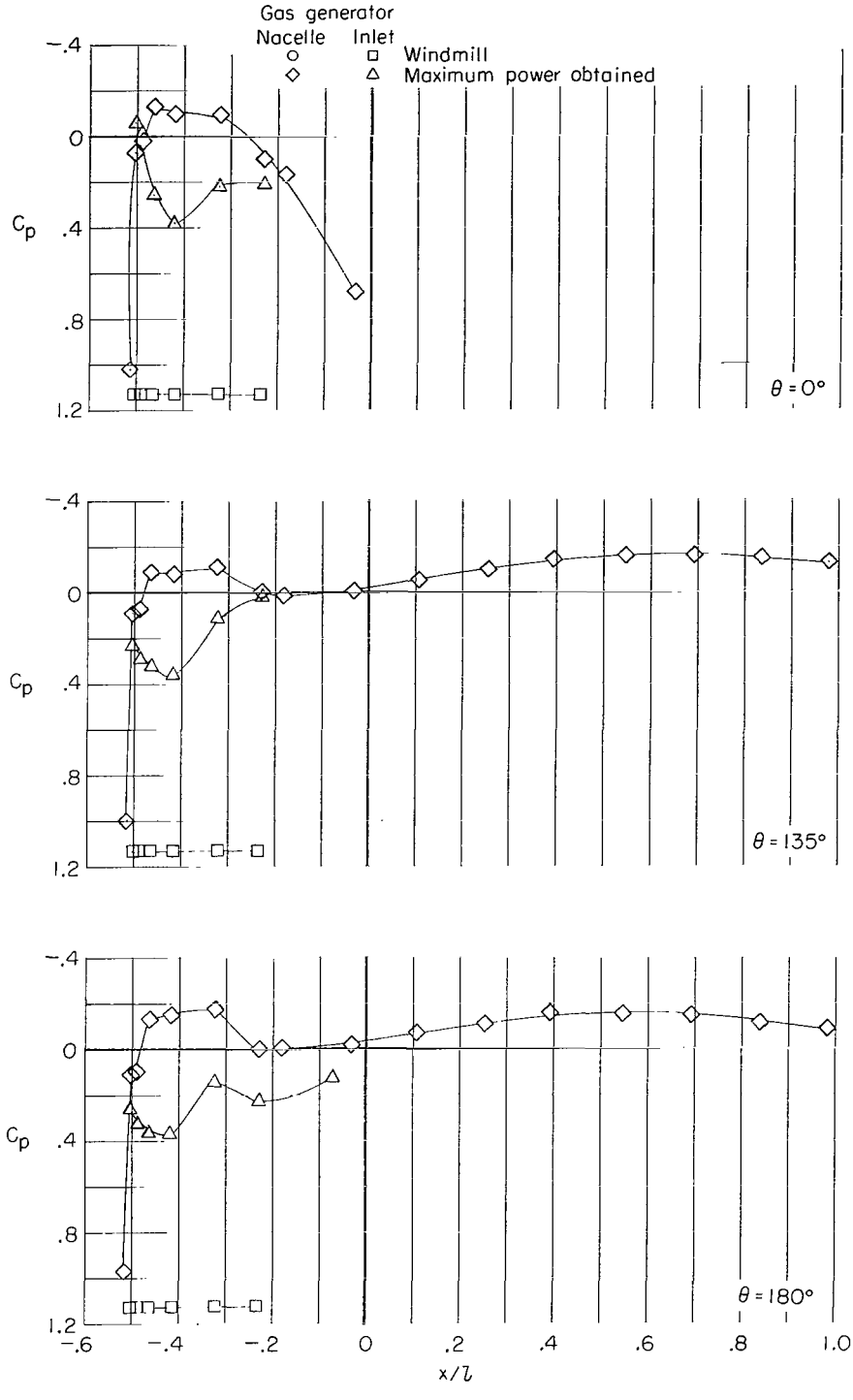

(a) $\alpha = -2^0$.

Figure 12.- Gas-generator-inlet and nacelle pressure distributions at M = 0.30.

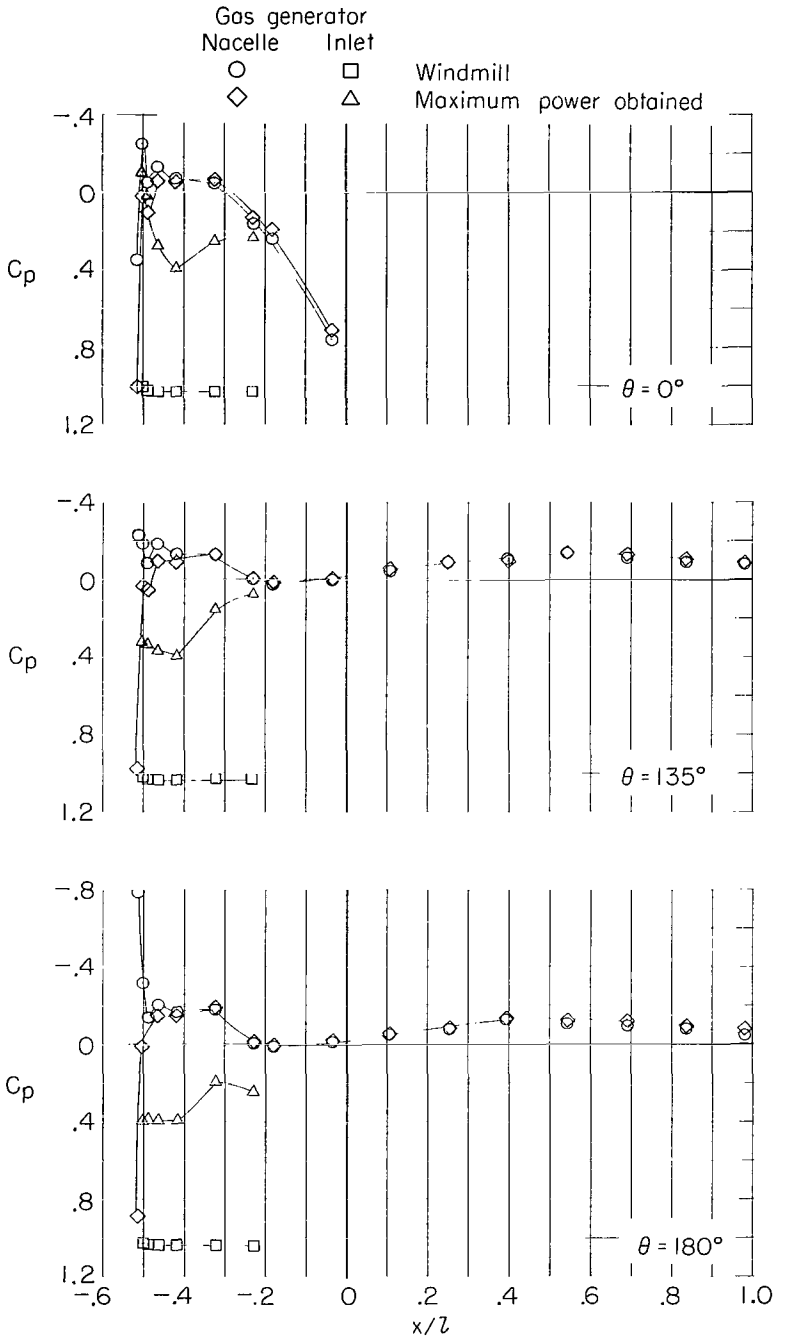

(b) $\alpha = 0^0$.

Figure 12.- Continued.

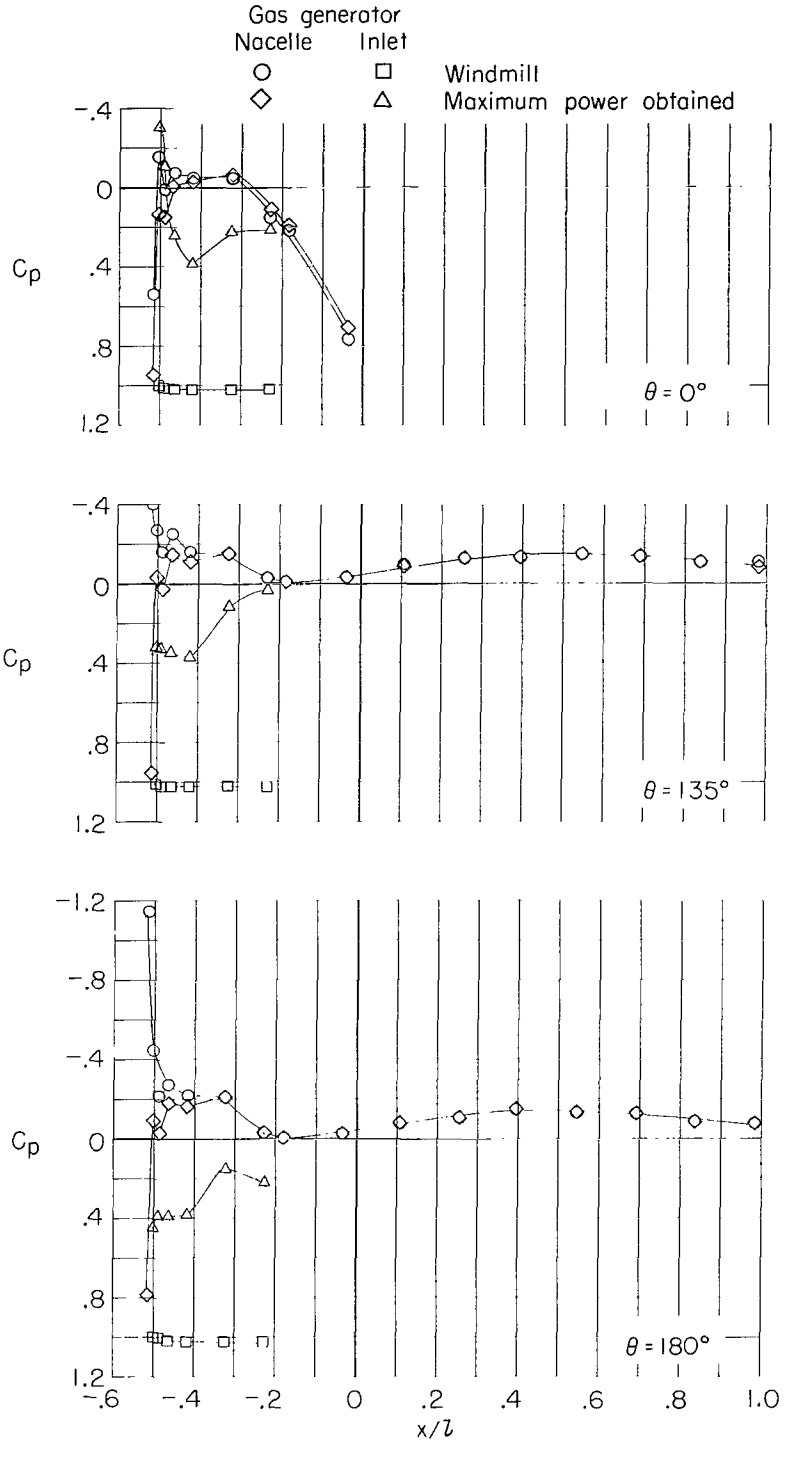

(c) $\alpha = 2^0$.

Figure 12.- Continued.

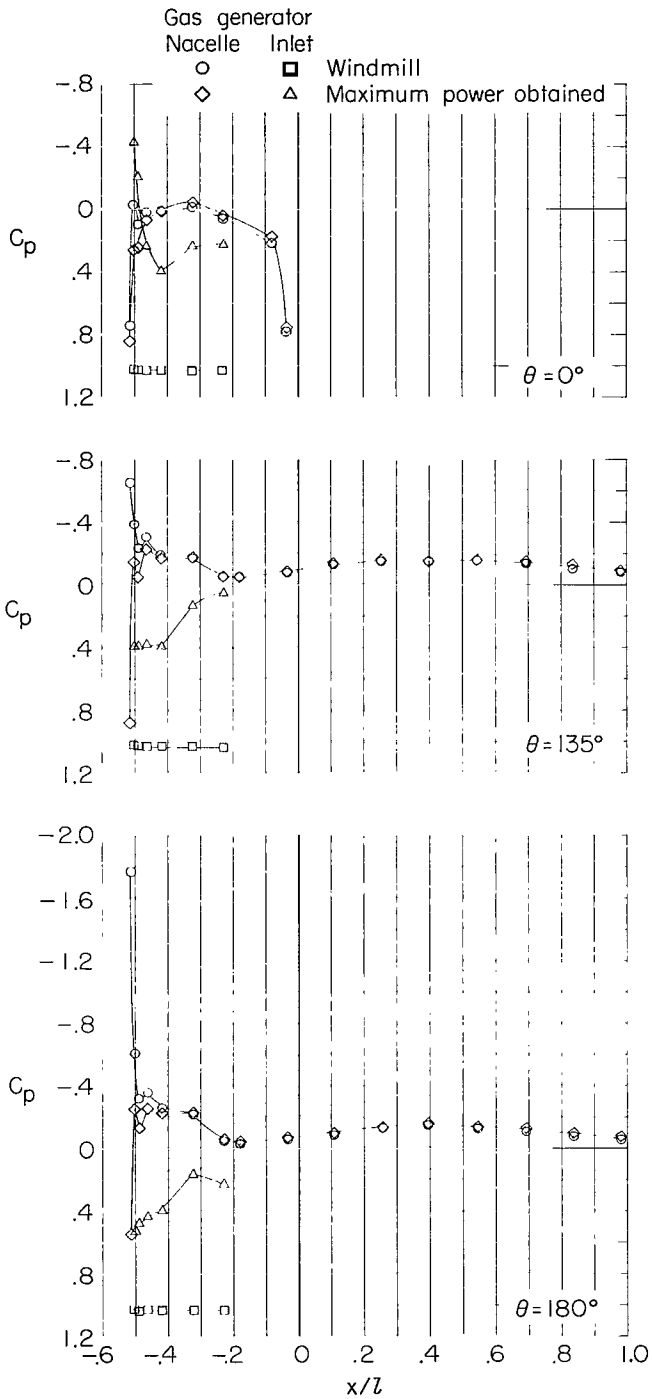

(d) $\alpha = 5^0$.

Figure 12.- Continued.

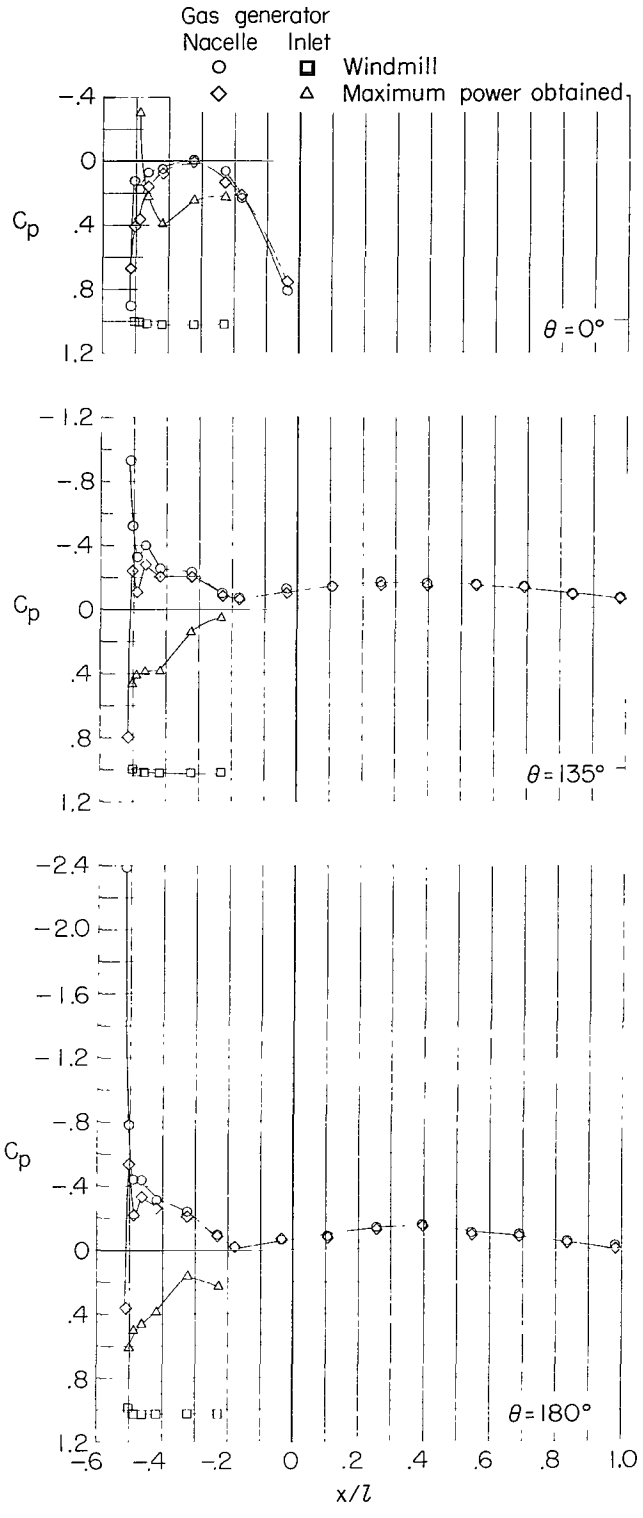

(e) $\alpha = 8^0$.

Figure 12.- Concluded.

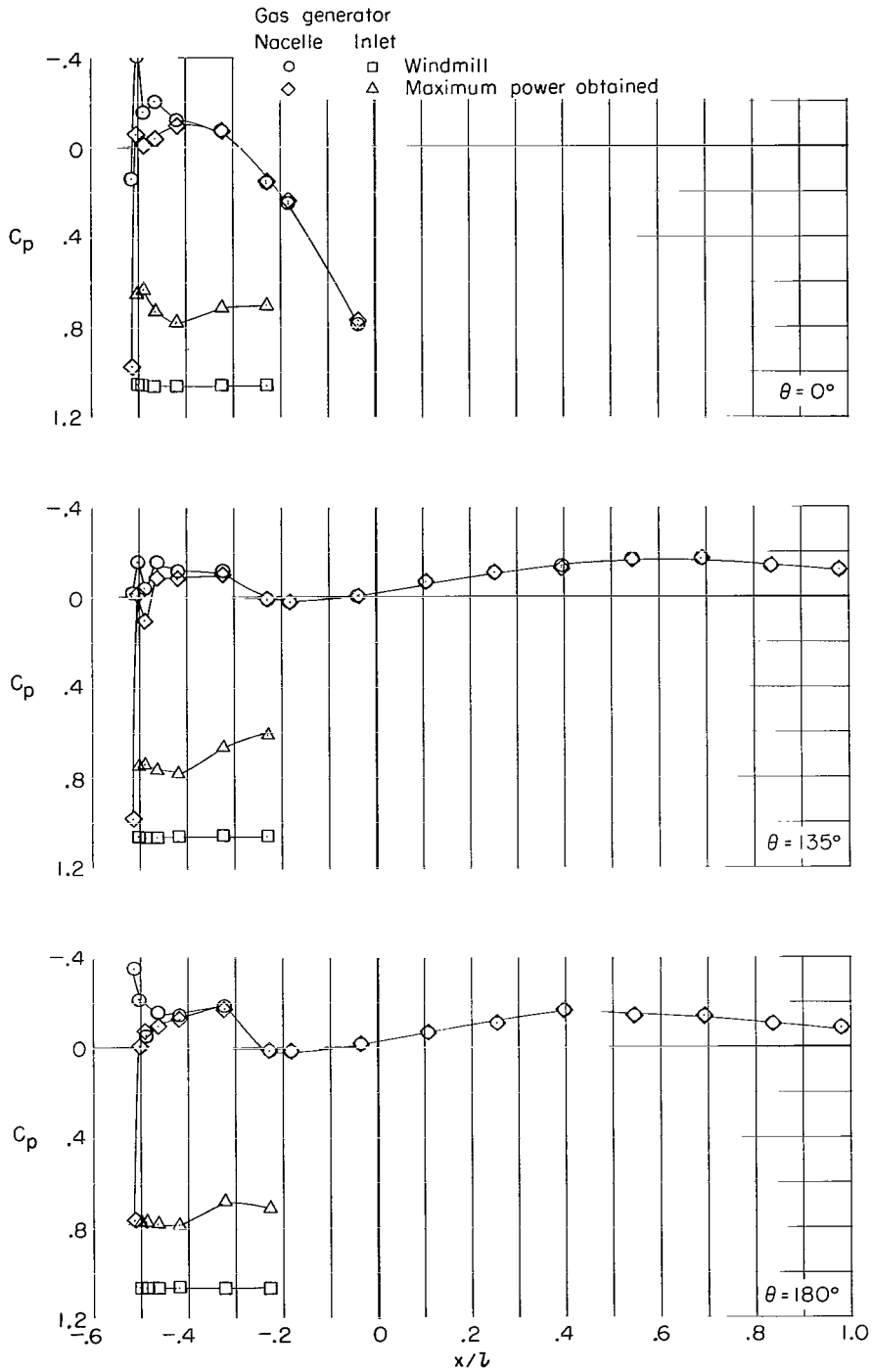

(a) $\alpha = -2^0$.

Figure 13.- Gas-generator-inlet and nacelle pressure distributions at M = 0.50.

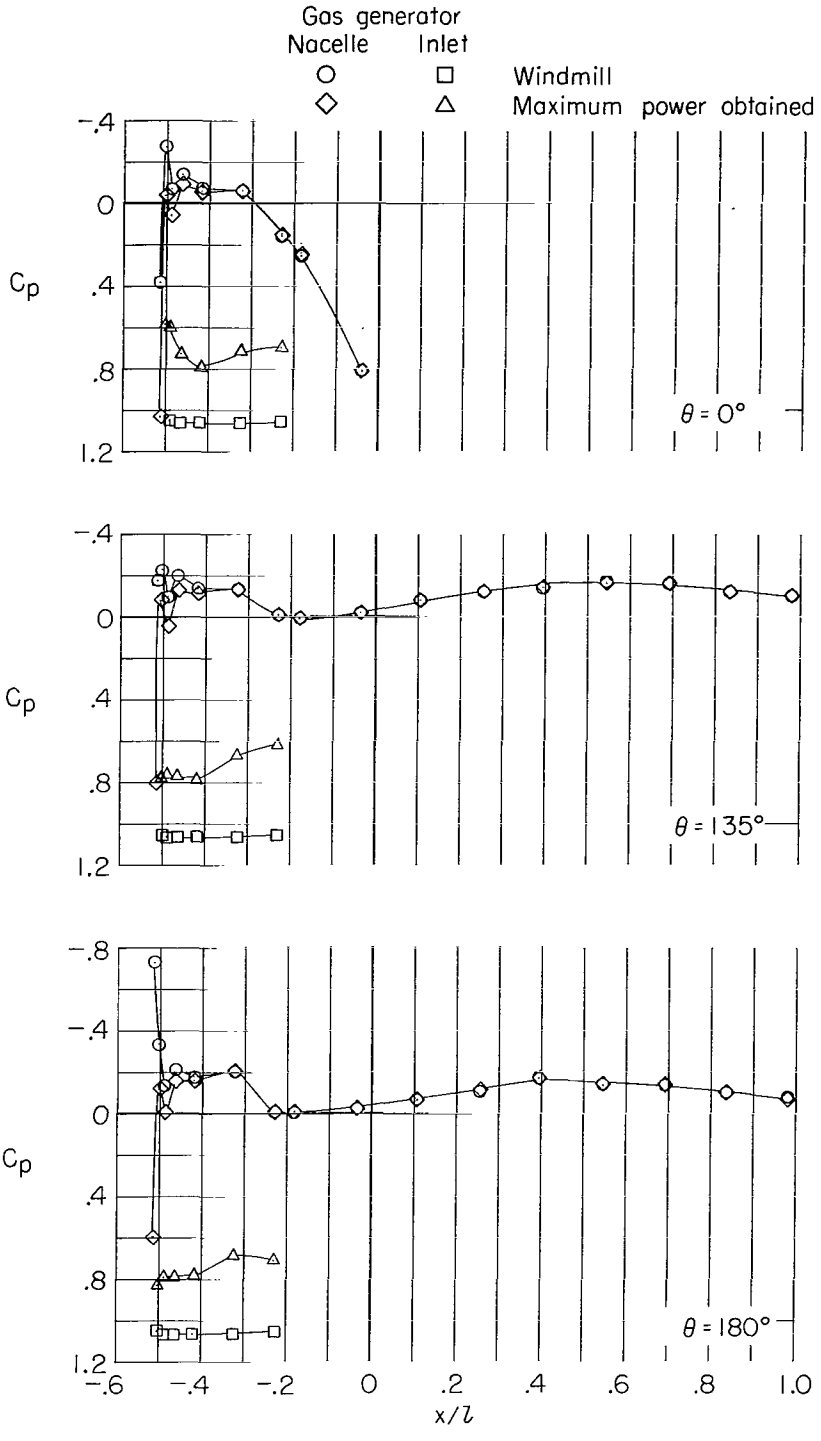

(b) $\alpha = 0^{o}$.

Figure 13.- Continued.

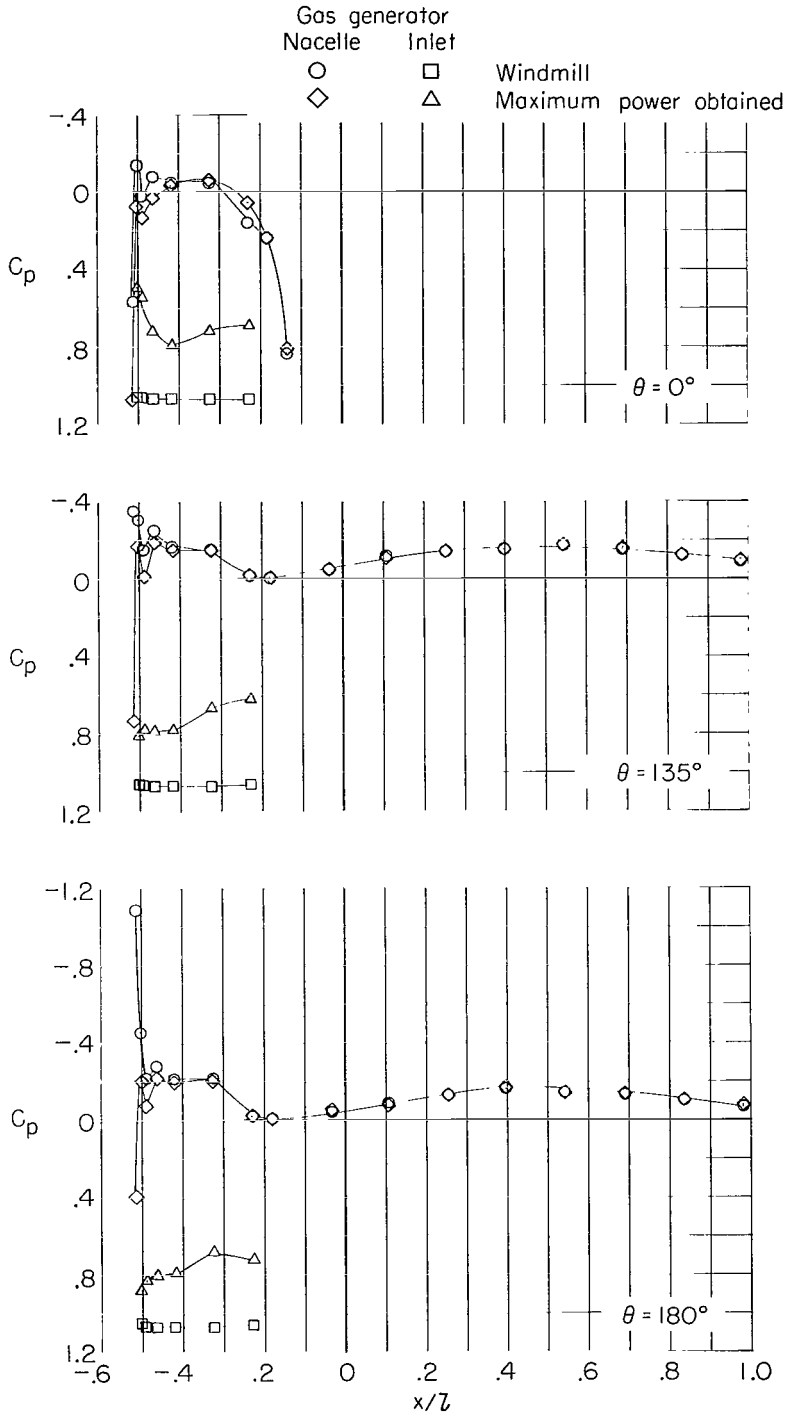

(c) $\alpha = 2^0$.

Figure 13.- Continued.

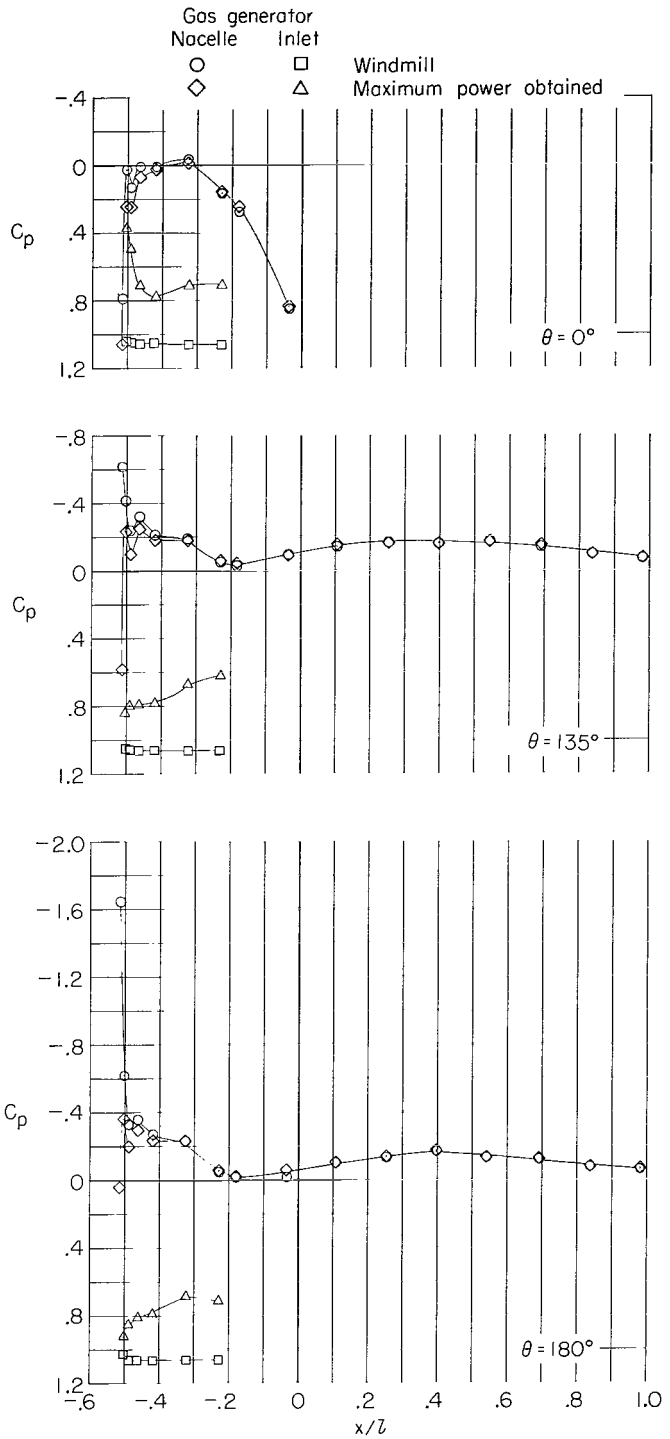

(d) $\alpha = 5^0$.

Figure 13.- Continued.

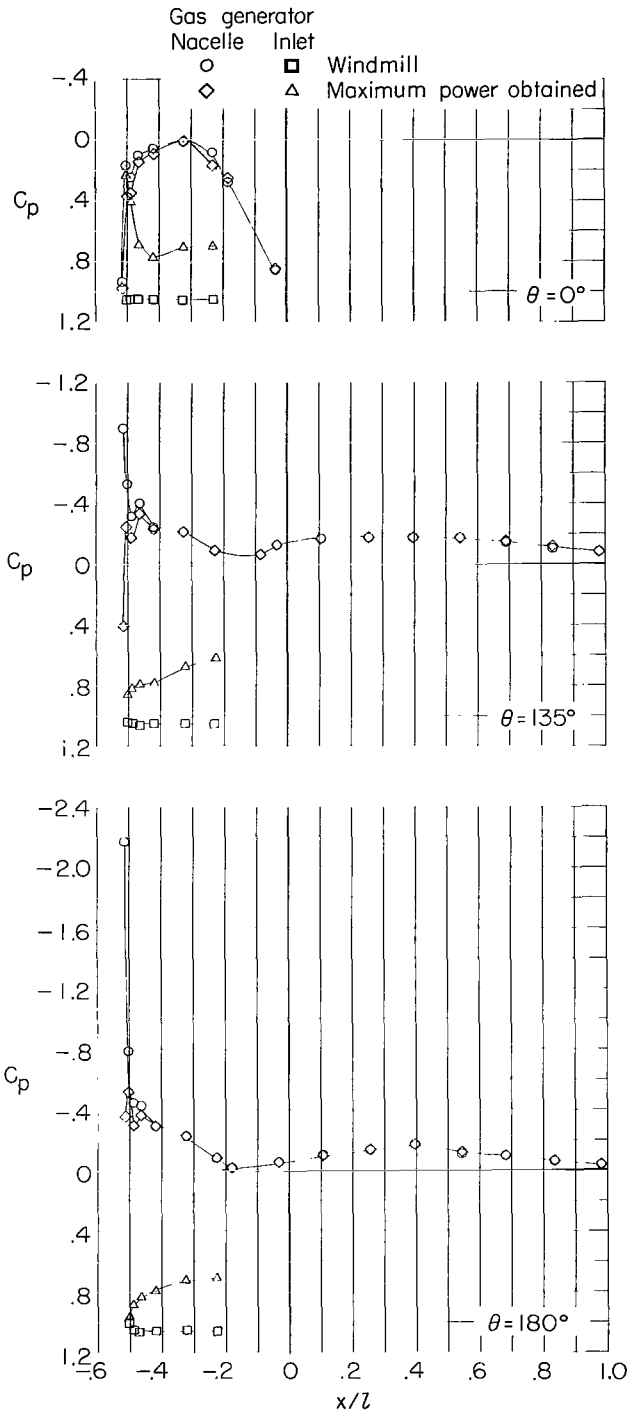

(e) $\alpha = 8^0$.

Figure 13.- Concluded.

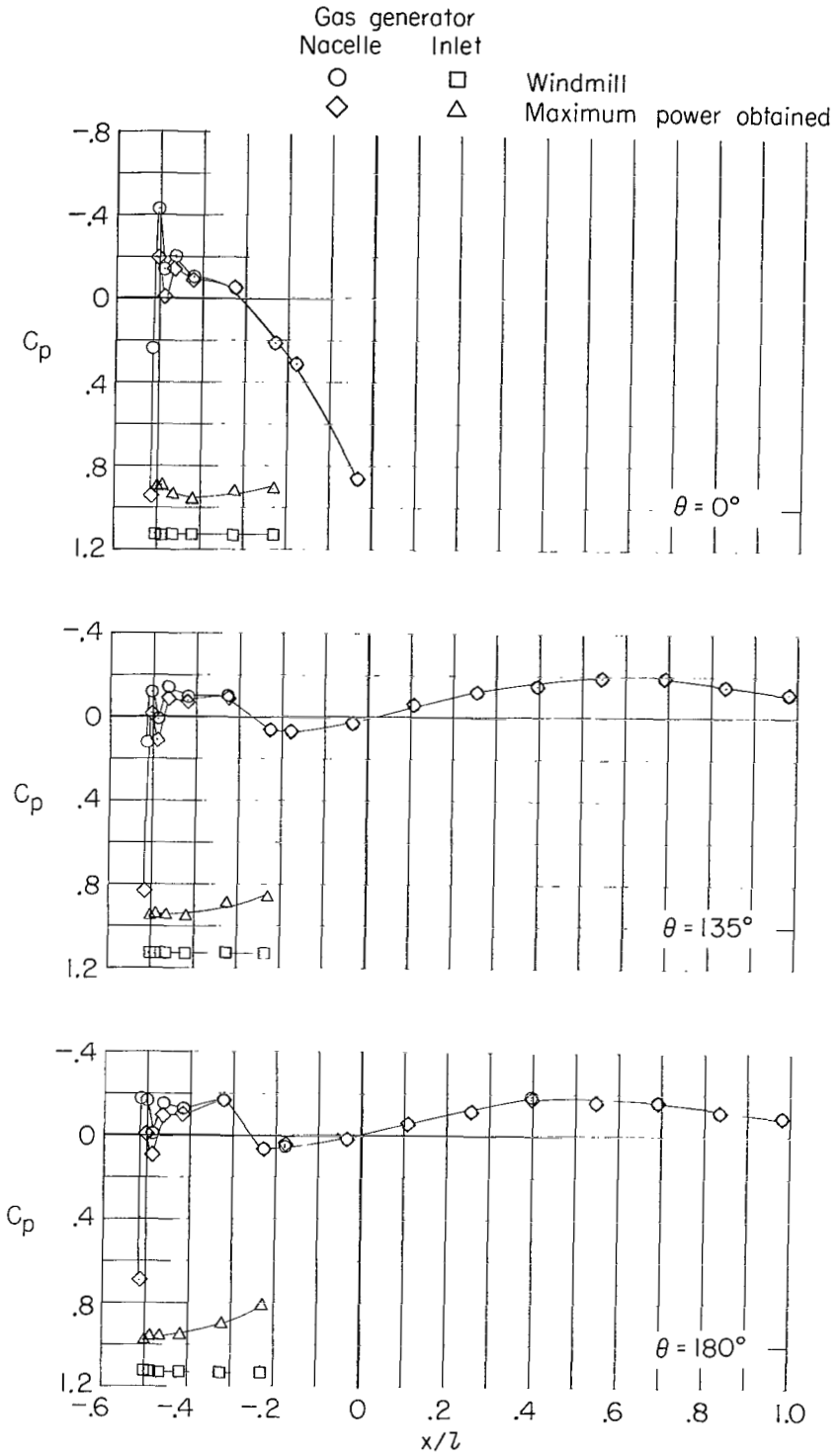

(a) $\alpha = -2^0$.

Figure 14.- Gas-generator-inlet and nacelle pressure distributions at M = 0.70.

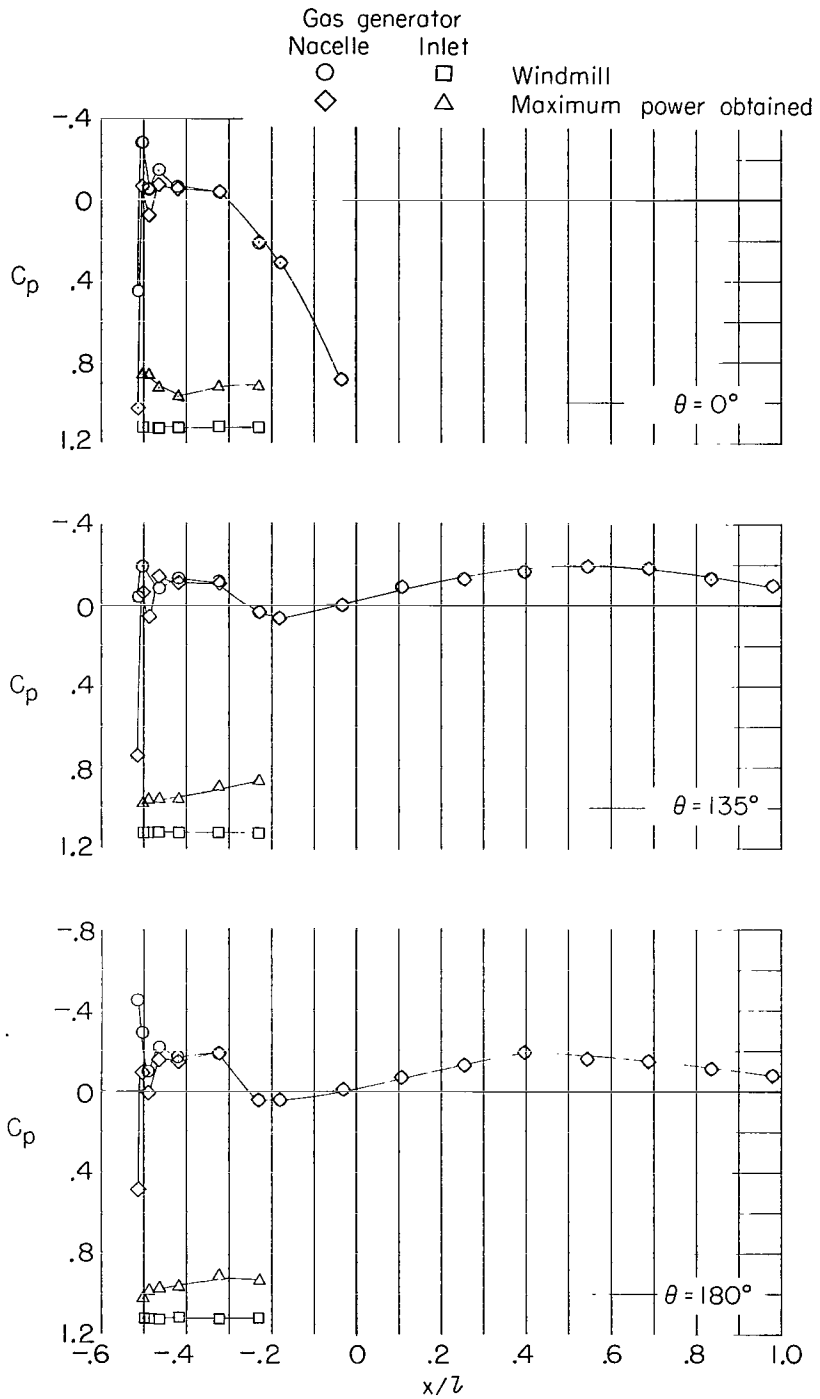

(b) $\alpha = 0^0$.

Figure 14.- Continued.

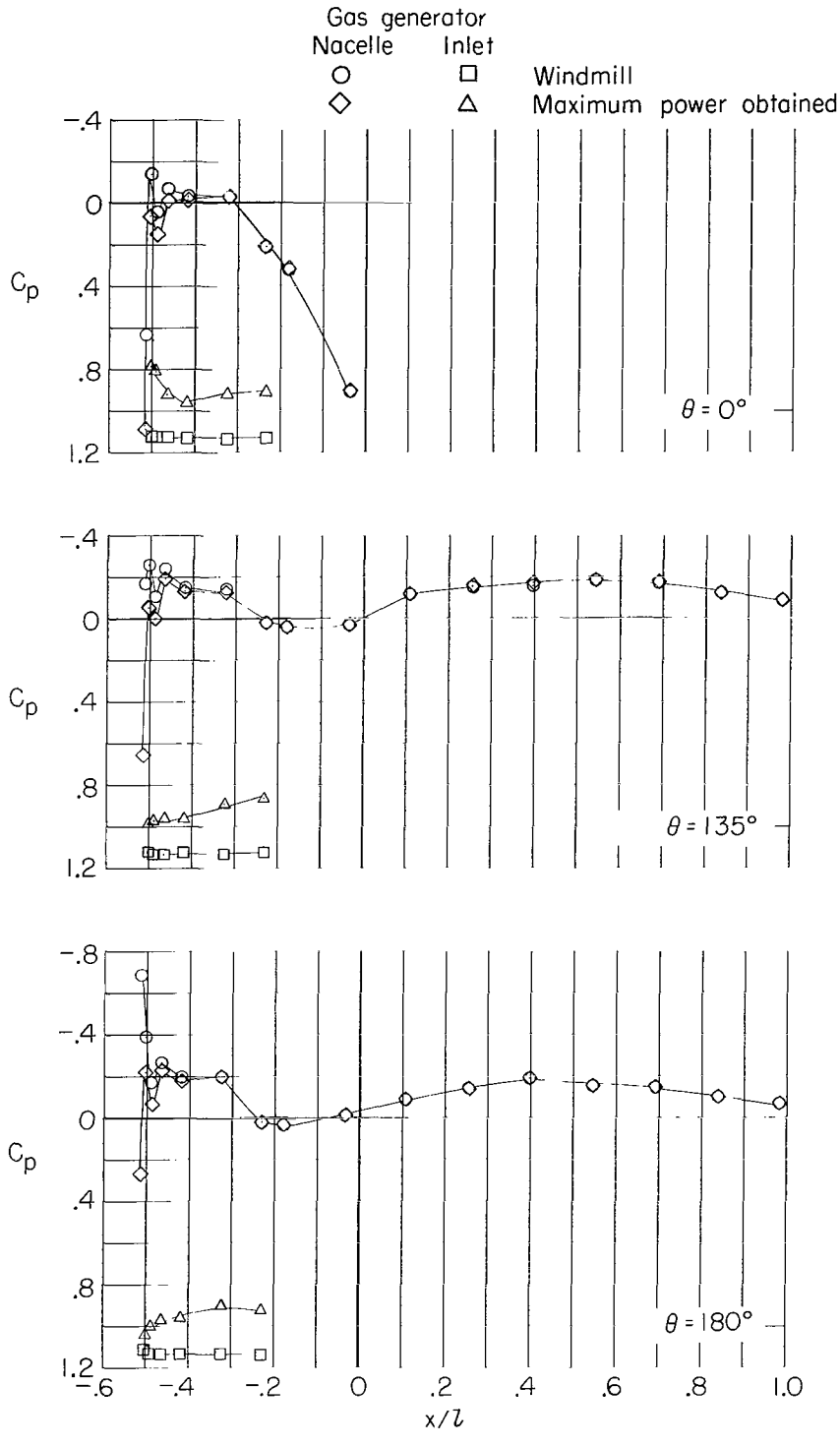

(c) $\alpha = 2^0$.

Figure 14.- Continued.

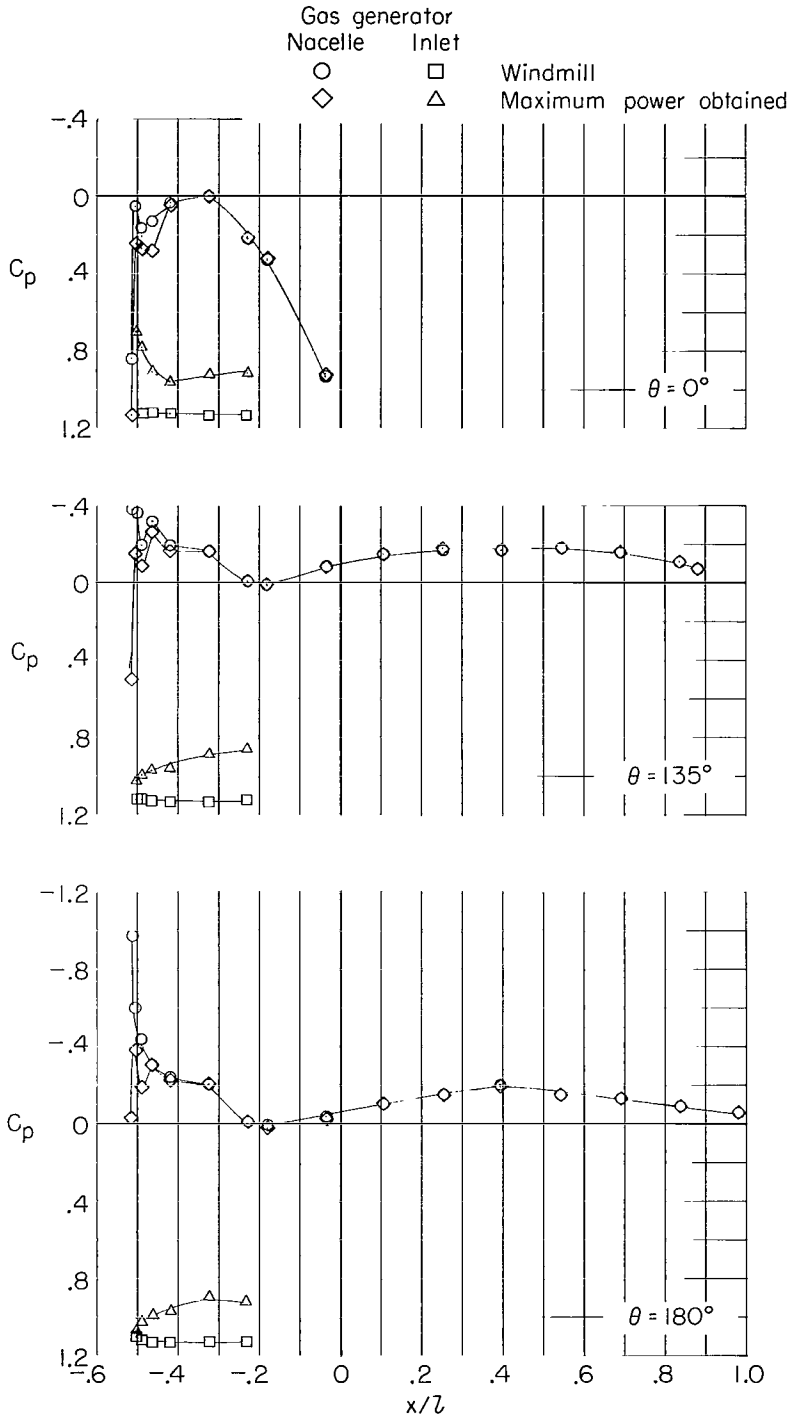

(d) $\alpha = 5^0$.

Figure 14.- Concluded.

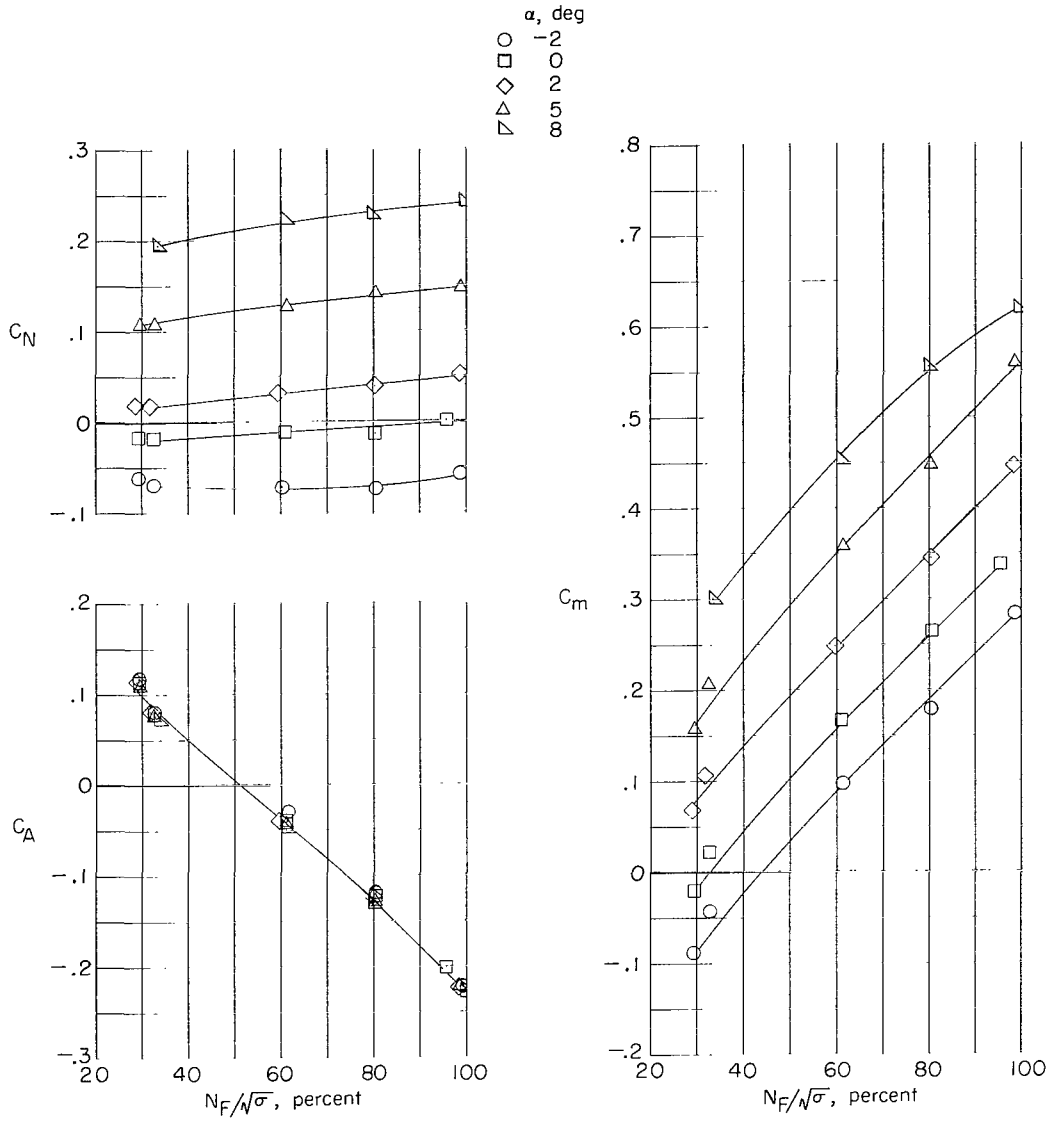

(a) M = 0.30.

Figure 15.- Variation of gross balance forces (thrust effects not removed) with corrected fan speed.

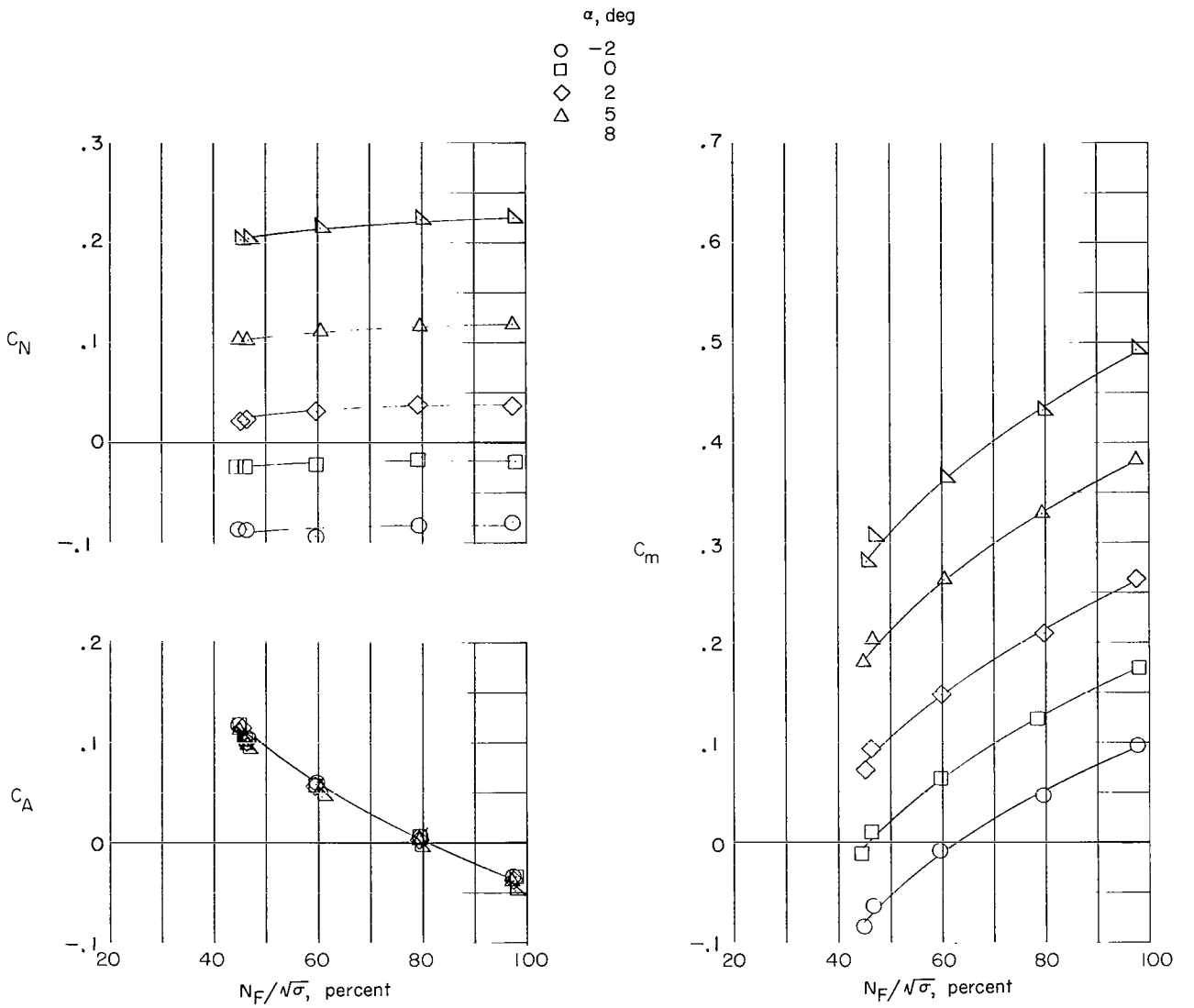

(b) M = 0.50.

Figure 15.- Continued.

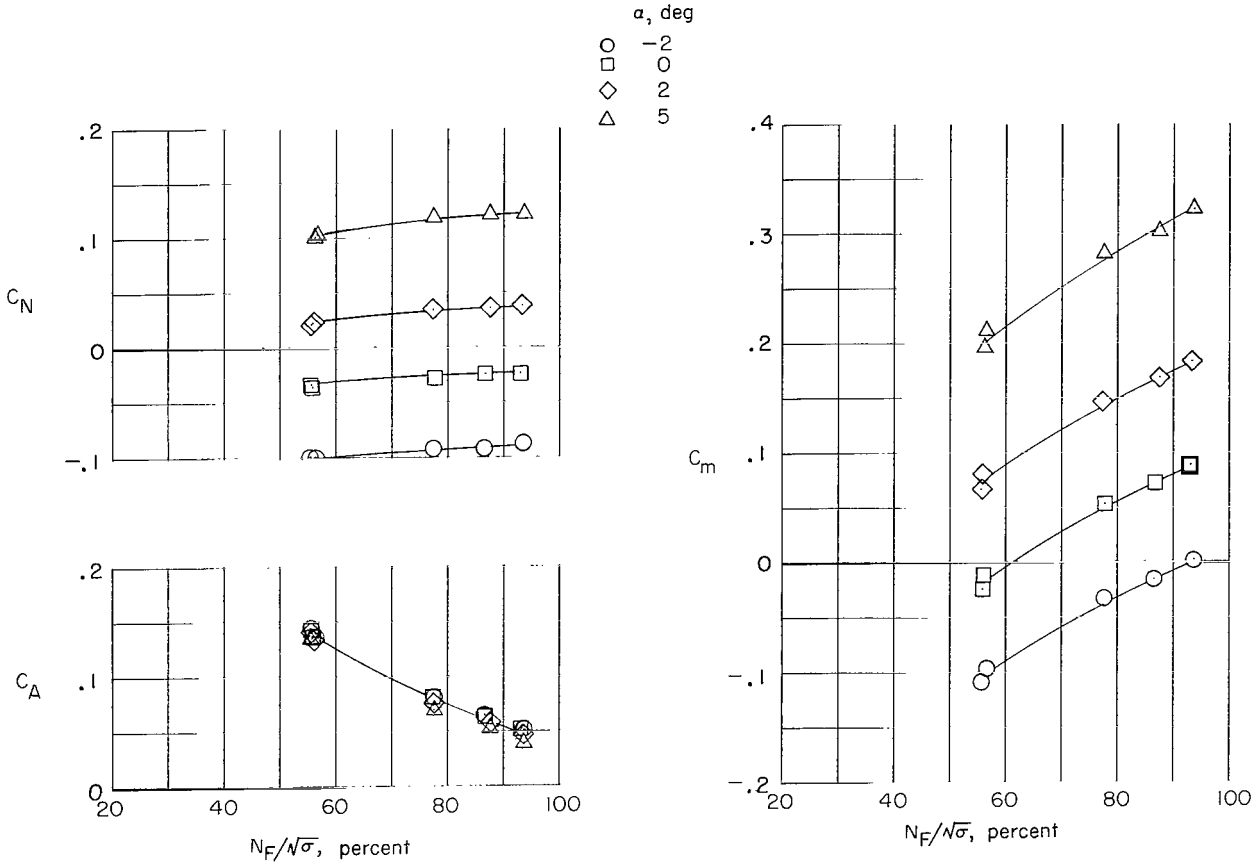

(c) M = 0.70.

Figure 15.- Concluded.

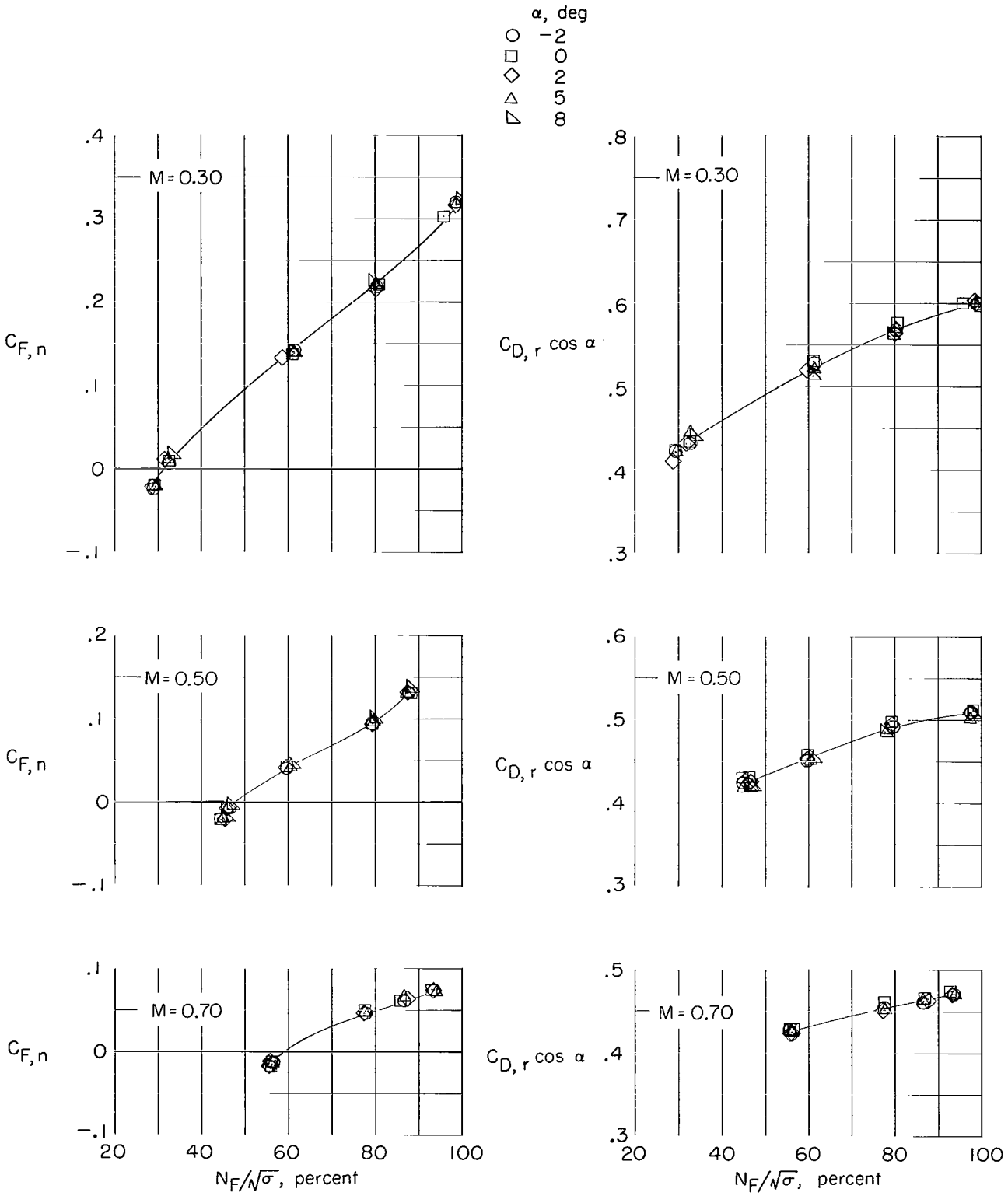

Figure 16.- Variation of net thrust coefficient and ram drag coefficient with corrected fan speed.

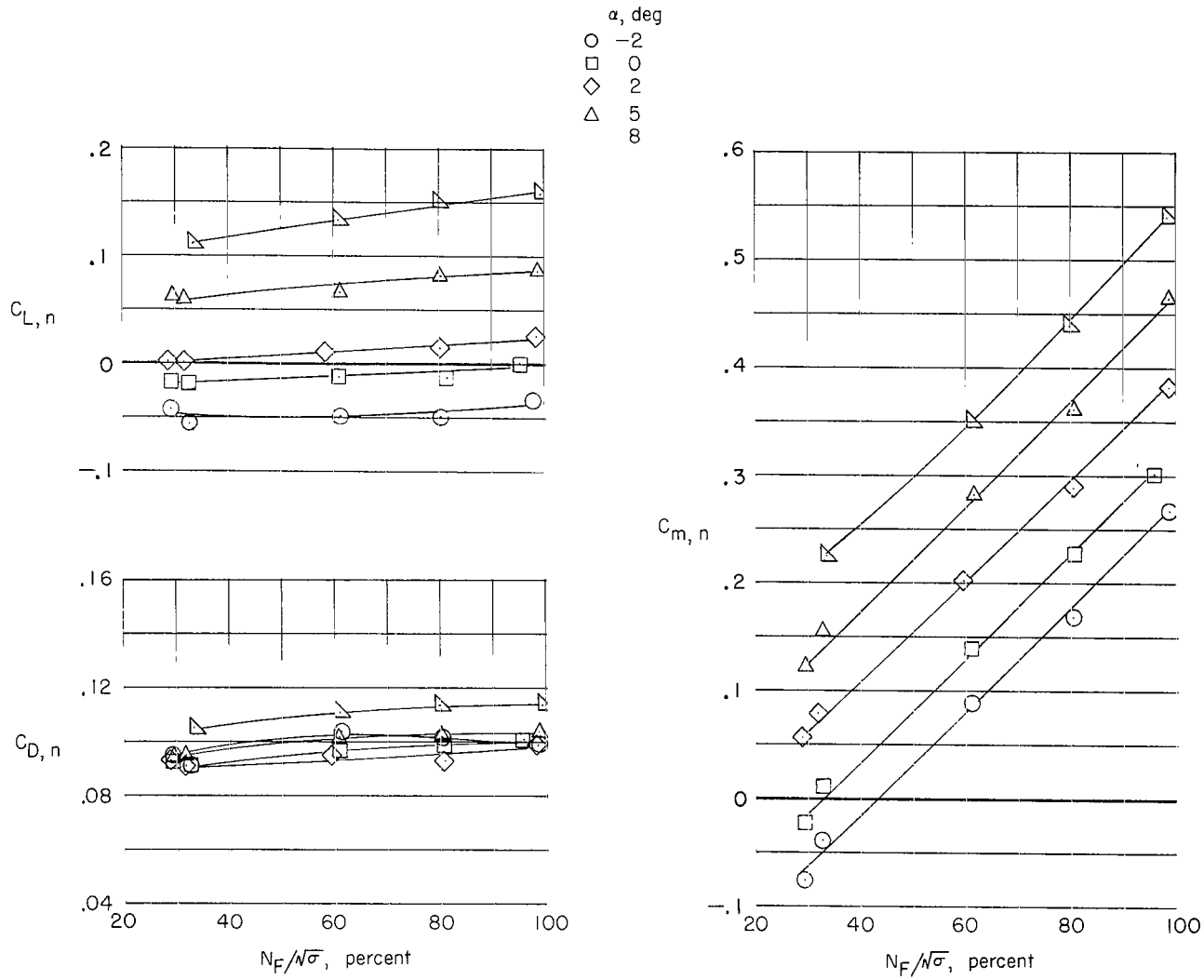

(a) M = 0.30.

Figure 17.- Variation of fan nacelle net aerodynamic forces (effects of thrust removed) with corrected fan speed.

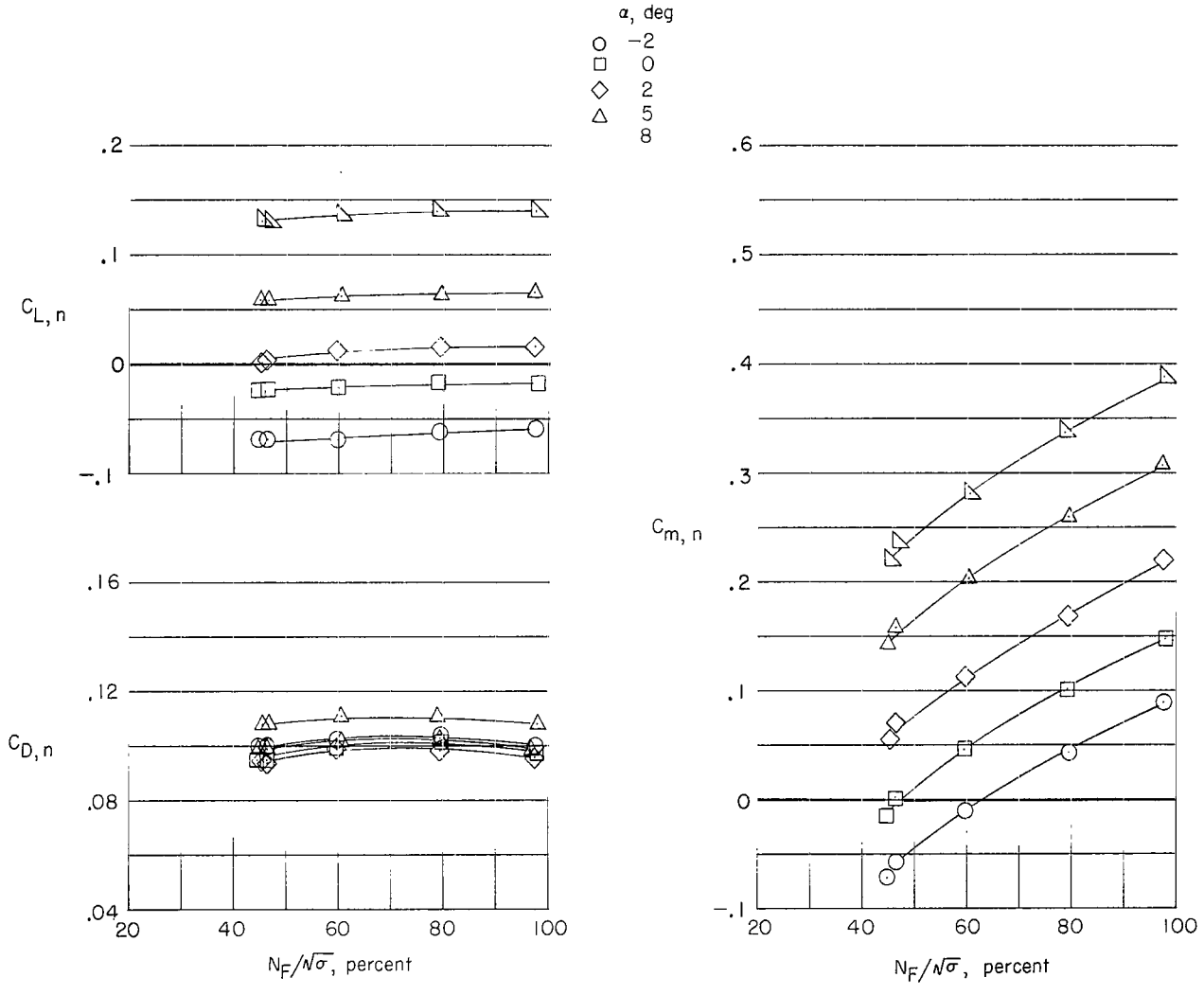

(b) M = 0.50.

Figure 17.- Continued.

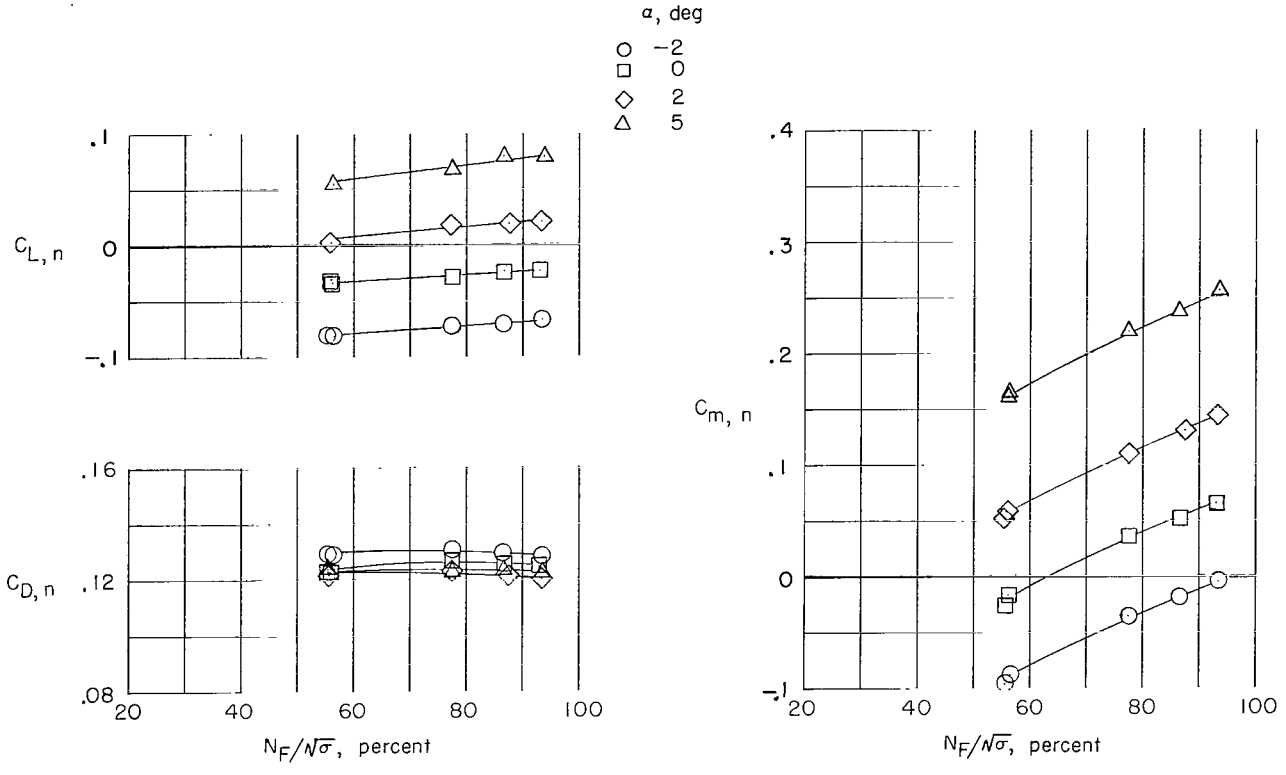

(c) M = 0.70.

Figure 17.- Concluded.

NASA-Langley, 1969 —— 28 L-6292